



VCU

Virginia Commonwealth University
VCU Scholars Compass

Theses and Dissertations

Graduate School

2021

IMAGING POTENTIAL IN SATURATION RECOVERY METHODS FOR SARCOIDOSIS PATIENTS WITH MEDICAL DEVICES

Samantha Zhao
Virginia Commonwealth University

Follow this and additional works at: <https://scholarscompass.vcu.edu/etd>



Part of the [Bioimaging and Biomedical Optics Commons](#)

© The Author

Downloaded from

<https://scholarscompass.vcu.edu/etd/6766>

This Thesis is brought to you for free and open access by the Graduate School at VCU Scholars Compass. It has been accepted for inclusion in Theses and Dissertations by an authorized administrator of VCU Scholars Compass. For more information, please contact libcompass@vcu.edu.

IMAGING POTENTIAL IN SATURATION RECOVERY METHODS FOR SARCOIDOSIS PATIENTS WITH MEDICAL DEVICES

A thesis submitted in partial fulfillment of the requirements for the degree of
Master of Science in Biomedical Engineering at Virginia Commonwealth University.

By

SAMANTHA ZHAO

B.S. Biomedical Engineering, Virginia Commonwealth University, 2020

Faculty Advisor: Jennifer Jordan, Ph.D., M.S.
Assistant Professor, Department of Biomedical Engineering and Pauley Heart Center
Director, Cardiovascular MRI Core Lab

Virginia Commonwealth University
Richmond, Virginia
August 2021

Table of Contents

Acknowledgement	4
Table of Figures	5
Table of Tables	7
Table of Equations	8
Abbreviations	9
Abstract	11
1 Background	12
1.1 Introduction to Cardiac MRI	12
1.2 Introduction to Cardiac Sarcoidosis	13
1.3 Current Methods and Short Comings for the CMR Assessment of Myocardial Scar	15
1.3.1 Late-Gadolinium Enhancement	15
1.3.2 Modified Look-Locker Inversion Recovery (MOLLI)	16
1.3.3 Saturation Recovery Single-Shot Acquisition	18
1.4 Gradient Echo Sequence Readouts	19
1.4.1 Balanced Steady-State Coherent Gradient Echo	20
1.4.2 Incoherent “Spoiled” Gradient Echo Sequence	20
1.5 Degradation in Diagnostic Image Quality Due to Implanted Cardiovascular Electronic Devices in Cardiac Sarcoidosis Patients	21
1.6 Specific Aims and Objectives	23
2 Quantitative T1-Mapping and Analysis	25
2.1 Rationale and Hypotheses	25
2.2 Methods	26
2.2.1 Study Design	26
2.2.2 CMR Protocol	27
2.3 Qualitative Analysis	28
2.4 Quantitative Analysis	30
2.5 Statistical Analysis	30
2.6 Results	31
2.6.1 Determination of Image Quality Between Methods	32
2.6.2 Analysis of Native T1-Values	34
2.7 Discussion	41

2.8	Limitations	43
2.9	Conclusion	43
3	Ancillary Analysis	44
3.1	Post Contrast T1 Considerations.....	45
3.2	Segmental Considerations.....	49
3.3	T2 Considerations	55
3.4	An In-Depth Look: A Head-to-Head Comparison.....	56
3.5	Future Directions	59
4	References.....	60

Acknowledgement

First, I would like to thank my advisor, Dr. Jennifer Jordan in the Department of Biomedical Engineering for her continued encouragement, guidance, and support throughout the past two years. I was never sure what I was getting into jumping into a masters' program and an accelerated one at that! In addition to a global pandemic, you helped pushed the research forward and keeping me on track. Her knowledge of biomedical sciences and clinical MRI were and continue to be indispensable not just for me, but for the entirety of VCU.

Next, I would like to thank Dr. John Wilson in the Department of Biomedical Engineering and Dr. Jordana Kron in the Department of Internal Medicine for serving on my committee. Their assistance was invaluable to the completion of this research. I would also like to give special thanks to Dr. Paul Wetzel and Dr. Thea Pepperl, both in the Department of Biomedical Engineering. Their coursework and dedication to education has led me to the path I take today and will continue forward with all their wisdoms.

Finally, I would also like to thank my mother, Kim Che, for always being a pillar in my life and educational journey. As single a mother, she has gone through thick and thin for putting four children through school. I couldn't have asked for a better mother and hope to continue to make you proud as I continue through my life's journey. Next, thank you to my grandmother, Choo Yueng Ling, for having raised me from infancy. Thank you to my siblings, Tiffany, Melissa, and Christopher, for providing your own unique forms of distraction and love.

Table of Figures

Figure 1. Comparison of T1-mapping sequences including MOLLI, shMOLLI, SASHA, and Saturation Pulse Prepared Heart-Rate Independent Inversion Recovery (SAPPHIRE).....	19
Figure 2. Localizer scan with severe artifact for participant two. As a result, participant two was not included in analysis.....	32
Figure 3. Image quality score distribution between SASHA and MOLLI scans of the heart. Slice-based scores were averaged from segmental scoring in pre-contrast scans.....	33
Figure 4. Distribution of slice-based image quality scores among the four methods: SASHA TRUFI, MOLLI TRUFI, SASHA FLASH, and MOLLI FLASH in pre-contrast scans.....	33
Figure 5. Comparison of global initial and secondary T1-values across the four methods. Student's t-test p-value result is reported.....	38
Figure 6. Graphical representation of global ANOVA test done between SASHA TRUFI, SASHA FLASH, MOLLI TRUFI, and MOLLI FLASH in pre-contrast scans.....	39
Figure 7. Graphical representation of slice-based ANOVA results between SASHA TRUFI, SASHA FLASH, MOLLI TRUFI, and MOLLI FLASH in pre-contrast scans.....	39
Figure 8. Tukey-Kramer results showing variations between the four methods and their q-values for native T1-values.....	40
Figure 9. Image quality score distribution between SASHA and MOLLI scans of the heart. Slice-based scores were averaged from segmental scoring in post-contrast scans.....	45
Figure 10. Distribution of slice-based image quality scores among the four methods: SASHA TRUFI, MOLLI TRUFI, SASHA FLASH, and MOLLI FLASH in post-contrast scans.....	46
Figure 11. Graphical representation of global ANOVA test done between SASHA TRUFI, SASHA FLASH, MOLLI TRUFI, and MOLLI FLASH in post-contrast scans.....	47
Figure 12. Graphical representation of slice-based ANOVA results between SASHA TRUFI, SASHA FLASH, MOLLI TRUFI, and MOLLI FLASH in post-contrast scans.....	48
Figure 13. Tukey-Kramer results showing variations between the four methods and their q-values for post-contrast T1-values.....	48
Figure 14. Image quality score distribution between SASHA and MOLLI segmental scans within the heart in pre-contrast values. Results are a combination of all readouts.....	50
Figure 15. Distribution of segmental image quality scores among the four methods: SASHA TRUFI, MOLLI TRUFI, SASHA FLASH, and MOLLI FLASH in pre-contrast values.....	50

Figure 16. Image quality score distribution between SASHA and MOLLI segmental scans within the heart in post-contrast values.....	51
Figure 17. Distribution of segmental image quality scores among the four methods: SASHA TRUFI, MOLLI TRUFI, SASHA FLASH, and MOLLI FLASH in post-contrast values.....	52
Figure 18. Graphical representation of segmental ANOVA results between SASHA TRUFI, SASHA FLASH, MOLLI TRUFI, and MOLLI FLASH in pre-contrast scans.....	53
Figure 19. Tukey-Kramer results showing variations between the four methods and their q-values for segmental, native T1-values.....	53
Figure 20. Graphical representation of segmental ANOVA results between SASHA TRUFI, SASHA FLASH, MOLLI TRUFI, and MOLLI FLASH in post-contrast scans.....	54
Figure 21. Graphical representation of slice-based ANOVA results between TRUFI and FLASH readouts using T2 values.....	56
Figure 22. Graphical representation of segmental ANOVA results between TRUFI and FLASH readouts using T2 values.....	56
Figure 23. IQS scores for participant 5.....	57
Figure 24. ANOVA results for participant five.....	58
Figure 25. Tukey-Kramer results showing variations between the four methods and their q-values in participant five.....	58

Table of Tables

Table 1. Visual and written criteria for image quality scoring for quantitative T1-values.	29
Table 2. Patient demographic and characteristics.	31
Table 3. Global and slice-based coefficient of variance and T1-values (ms) for all participants for the basal (B), mid-cavity (M), and apical (A) slices.	35

Table of Equations

Equation 1. T2-decay.....	12
Equation 2. T1-relaxation.....	12

Abbreviations

American Heart Association	(AHA)
Analysis of variance	(ANOVA)
Balanced fast field echo	(Balanced FFE)
Balanced steady-state free precession	(bSSFP)
Cardiovascular implantable electronic device	(CIED)
Cardiovascular magnetic resonance	(CMR)
Coefficient of variation	(CoV)
C reactive protein	(CRP)
Cardiac sarcoidosis	(CS)
Computed tomography	(CT)
Degrees of freedom	(df)
Extracellular volume	(ECV)
Fast imaging employing steady-state acquisition	(FIESTA)
Fast low angle shot	(FLASH)
Gradient echo	(GRE)
Image quality score	(IQS)
Late gadolinium enhancement	(LGE)
Motion-corrected	(MOCO)
Modified Look-Locker inversion	(MOLLI)
Multiplanar gradient-recalled	(MPGR)
Magnetic resonance imaging	(MR)
Magnetic resonance imaging	(MRI)
Magnetization transfer	(MT)
Positron emission tomography	(PET)
Phase-sensitive inversion recovery	(PSIR)
Critical value	(q_{crit})
Radio frequency	(RF)

Saturation Pulse Prepared Heart-Rate Independent Inversion Recovery	(SAPPHIRE)
Saturation recovery single-shot acquisition	(SASHA)
Shortened MOLLI	(shMOLLI)
Signal to noise ratio	(SNR)
Saturation recovery	(SR)
Single shot	(SS)
Steady-state free precession	(SSFP)
Tesla	(T)
True fast imaging with steady-state precession	(TRUFI)
Wideband LGE	(WB LGE)
Work in progress	(WIP)

Abstract

Cardiovascular magnetic resonance (CMR) imaging is a preferred imaging methodology due to its lack of ionizing radiation and ability to detect myocardial inflammation and fibrosis using quantitative T1 mapping techniques. Cardiac sarcoidosis (CS) is characterized as the formation of granulomas in the myocardium. Current methods for detection include measuring non-cardiac specific C-reactive protein (CRP) levels, or PET imaging, which uses ionizing radiation, therefore CMR would make an ideal imaging option. However, many CS patients have implanted cardiac devices which can cause degradation in image. The modified Look-Locker inversion recovery (MOLLI) method is widely used in quantitative T1 mapping with high precision but low accuracy and susceptibility to artifact. Newer methods like saturation recovery single-shot acquisition (SASHA) may be less susceptible to field inhomogeneities but have yet to be compared directly to MOLLI in CS patients with implanted devices. T1-values can further be affected by how the signal data is compiled, or their readout. Common readouts include balanced steady-state free precession (TRUFI) and fast low angle shot (FLASH).

First, SASHA sequences provided more consistent images that can be used for diagnostic purposes while MOLLI varied between extreme image quality categories. Finally, SASHA techniques in general show lower variability while GRE readouts suggest higher reproducibility between multiple scans. Through this sub-analysis study, SASHA TRUFI, MOLLI TRUFI, SASHA FLASH, and MOLLI FLASH sequences were optimized to move forward with primary studies of CS patients in the MRI field.

1 Background

1.1 Introduction to Cardiac MRI

Magnetic resonance imaging (MRI) is on the forefront of imaging modalities. MRI manipulates the abundance of positive protons from water in the human body to create detailed images of organs and tissues. Patients are placed in a powerful magnetic field to be scanned in the range of 1-3 Tesla (T) whereas the Earth's natural magnetic field is around 30uT (1).

While inside the machine, protons within the body are aligned parallel to the magnetic field B_0 . A gradient coil can be used to produce a linear variation of the magnetic field known as B_1 . Radio frequency (RF) pulses, typically 90 degrees, are applied to the area of interest to disrupt the aligned protons. When the protons revert to their magnetized positions, they release radio signals that are picked up by receivers (1, 2).

Directly after the RF pulse is the peak of the transverse signal. At about 1/3 of the peak is known as the T2 relaxation time as described in **Equation 1**. This is also known as the T2 decay value as the function decreases exponentially (3).

$$M_{xy}(t) = M_0 e^{\frac{-t}{T_2}}$$

Equation 1. T2-decay.

Longitudinal recovery that begins after the excitation pulse is described by **Equation 2**. The T1 relaxation time is characterized by about 2/3 of full recovery (3).

$$M_z(t) = M_0 (1 - e^{-\frac{t}{T_1}})$$

Equation 2. T1-relaxation.

The time for recovery along the z-axis is known as T1 or longitudinal relaxation time. The relaxation time from the x- and y-axis are known as T2 or transverse relaxation times.

MRI is shown to capably differentiate between soft tissues by taking advantage of the ranges of T1 and T2 values, especially those involved in the heart. Approximate T1 values at 1.5T for fat and water are 260ms and 4000ms respectively. T2 values for fat and water are approximately 80ms and 2000ms (1). Without any enhancement, these are known as native T1 and T2 values. Similarly, healthy myocardial tissue will have different T1 and T2 properties than pathologic myocardial tissues allowing for quantitative analysis (4, 5).

Cardiovascular magnetic resonance (CMR) imaging is specifically designed to analyze pathology and morphology of the heart. This includes but is not limited to tissue characterization, blood flow, and myocardial perfusion. CMR is particularly useful in diagnosis of the heart including cardiomyopathies, like scarring of the heart, compared to other imaging modalities such as x-ray, positron emission tomography/computed tomography (PET/CT), or fluoroscopy (1, 6). This is in part due to the use of magnetic fields and RF pulses in CMR as compared to harmful ionizing radiation that may result in burns, genetic damage, or increase in risk projection (1, 7, 8).

1.2 Introduction to Cardiac Sarcoidosis

Myocardial tissue can be affected by a variety of pathologies. Inflammation of the heart muscle, or myocarditis, can affect the heart's ability to pump blood in response to viral infections (9, 10). Another inflammatory disease is cardiac sarcoidosis (CS): the development of granulomas or inflammatory cells in the body. Current surveillance methods include monitoring the C reactive protein (CRP) which is a non-cardiac specific marker of inflammation. Other imaging modalities like PET/CT use low doses of radiation put into the patient's body. This process may be expensive

and difficult to prepare for. Constant exposure to radiation may lead to long term adverse health effects like cancer or cardiovascular disease. Identification of myocardial inflammation and scarring due to CS is extremely important as they can lead to complications further in life. Thickened myocardium makes it harder to pump blood as the tissue loses its elasticity. Abnormal heart rhythms are especially alarming and need to be addressed. Cardiac edema is characterized by swelling of the heart. Excess fluid, in this case blood, builds up in the right ventricle, causing it to swell and decrease overall blood (11, 12). Another case to consider is myocardial scarring. This is an accumulation of fibrosis tissue due to disease or trauma. The result from an injury where necrotic tissue transforms in fibromas are fibrosis. With the myocardium inflamed, the tissue becomes thicker and less elastic. This may result in reduced function of the heart leading to shortness of breath, fatigue, and arrhythmias (13-17).

Cases where scarring and inflammation are detected are typically given steroids as treatment. While steroids are effective at reducing inflammation, many other side effects due to long term use such as reduced immune response, muscle weakness, and mood swings (18, 19). Scar is found to be directly related to major adverse cardiovascular effects. Detection and quantification of the extent of myocardial scarring is important in early prognostic scans in addition to monitoring changes in current clinical management. While focal fibrosis may be easier to detect, it is the diffuse fibrosis that is more commonly overlooked (16, 17, 20, 21). In addition, diagnostic quality of scans can be inhibited by cardiovascular implantable electronic device (CIED) artifact.

CMR provides high spatial resolution, ability to assess normal myocardial wall thickness, and show the spread of nonviable myocardium within the heart. Above all, MRI is non-ionizing compared to other imaging modalities and painless compared to biopsy or surgery.

1.3 Current Methods and Short Comings for the CMR Assessment of Myocardial Scar

1.3.1 Late-Gadolinium Enhancement

To better characterize tissue, contrast agents like gadolinium are often administered to help better differentiate visually between normal and abnormal tissues by shortening T1 values. Gadolinium, a water-soluble, extracellular based contrast agent, is given to the patient and diffuses throughout the tissues providing high contrast in the extracellular volume and accumulates in other areas like interstitial fibrosis. The contrast agent accumulates in the proliferated fibroblasts therefore enhancing pathologies, visual contrast, and shortening T1 recovery time. Patients are placed in the scanner and given the contrast agent intravenously. After 5 to 10 minutes, late gadolinium enhancement (LGE) acquisition begins (22). LGE is considered the gold standard MRI sequence for identifying myocardial inflammation and focal fibrosis. Well-established LGE techniques are single shot (SS) or phase-sensitive inversion recovery (PSIR). SS is a technique where all data is acquired after a single 90-degree excitation pulse. PSIR is a common sequence offered by many MRI vendors that preserve the polarity of the longitudinal component of magnetization (1). These are images taken in one breath-hold if allowed by patient capabilities.

Patients usually referred for CMR typically have lower cardiac function, and therefore introduce many artifacts via motion during the scanning process or having an implanted device producing off-resonance artifacts. Overall, LGE sequences are not well equipped to deal with artifacts in images due to magnetization or implanted devices. LGE is also not entirely able to capture diffuse fibrosis for useful diagnostic value. In a study by Abdel-Aty et al., only 71% of LGE scans had diagnostic accuracy out of 25 patients suspected to have acute myocarditis (6). In another study to assess myocardial scar in patients with cardiovascular implanted devices, only 78% of scans were determined to be diagnostic (23).

To combat high frequency artifacts caused by things such as implanted devices, a wideband LGE (WB LGE) sequence was developed by increasing the spectral bandwidth of the RF pulse in traditional LGE to account for the frequency shifting of surrounding tissue. Typically, the spectral bandwidth is increased from 1.1kHz to 2-6kHz. The larger frequencies are typically those occupied by off resonant artifact due to CIEDs near the heart. WB LGE comparisons to traditional LGE are stark especially in patients with cardiac devices. Although there is resounding success in removing off-resonant artifact, it is still subject to partial image voids due to device leads, geometric distortions, and motion artifact.

In contrast to a previous study where 32% of traditional LGE scans were non-diagnostic, 100% of scans done with WB LGE were found to be without severe artifact where 79% of the patients had implanted defibrillators. This study also changed medical management in 49 out of 113 patients who previously only had traditional LGE scanning sequences (23). WB LGE has also shown to remove artifact from 87% (n=22) scans using a free-breathing motion-corrected (MOCO) sequence (24). Images with persisting hyper-enhancement artifact with standard LGE images had their artifact score reduced with WB LGE in 21 out of 27 patients (25). Additionally, Stevens et al. eliminated hyperintensity artifact in 16 of 18 patients using WB LGE (26). Importantly, despite the success of WB LGE, it remains subject to the limitation of not identifying diffuse fibrosis. Thus, quantitative T1 mapping methods are still needed to succinctly tell the difference between diffuse and focal fibrosis.

1.3.2 Modified Look-Locker Inversion Recovery (MOLLI)

Due to limitations from qualitative traditional LGE, methods of quantitative T1-mapping began to be developed and tested. One of the first techniques developed was the Look-Locker sequence which involves taking images repeatedly after inversion pulses to get multiple images along the

recovery curve. As an inversion recovery method, this completely magnetizes protons, and as they precess to normal, images are taken at specific inversion times to create a recovery curve. As a basic technique, it has some drawbacks including only apparent T1 values and in-plane and through-plane motion artifacts. As a result, the modified Look-Locker inversion (MOLLI) recovery method was derived. Rather than a qualitative assessment, this quantitative T1-mapping technique provides voxel-by-voxel T1 measurements. A widely used MOLLI sequence is a 5(3)3 sequence: 180-degree RF pulse followed by 5 images taken across 5 heart beats at varying inversion times afterwards a 3-heartbeat rest, another 180 degree pulse, and 3 more images taken at offset inversion times. This builds a recovery curve for each pixel of an image and results in a T1 map. MOLLI has been extensively studied and used in clinical settings. The sequence is known to have high precision and reproducibility. Although generally involving undervalued T1 values, MOLLI has been useful in assessing both focal and diffuse myocardial fibrosis. To reduce scan time and patient time in the magnet, a shortened MOLLI (shMOLLI) sequence was developed. The shMOLLI sequence decreases the breath hold time to 9 heartbeats. As expected, motion artifact is significantly reduced compared to standard MOLLI. Although as its foundations are still an inversion recovery, it is still susceptible to the same drawbacks of MOLLI.

Although generally high in image quality, there are still disadvantages to the inversion recovery methods. MOLLI is shown to have high dependence on T2 values, magnetization transfer (MT), and inversion efficiencies. Studies have shown that MT decreases measured T1 by 10% or greater. MT is the result of applied RF pulses to the interaction of bound proton pools spilling into the free water pool. Inversion efficiencies have been shown to be a source of T1 error as the pulses do not fully excite the area of interest. The conventional steady-state free precession (SSFP) readout of MOLLI-based methods is also highly susceptible to off-resonant errors in T1 values.

1.3.3 Saturation Recovery Single-Shot Acquisition

In contrast, there are saturation recovery methods that have been recently introduced for MRI and CMR uses. A saturation recovery (SR) method involves taking a single signal measurement at different inversion times across different heartbeats. A saturation recovery single-shot acquisition (SASHA) is a relatively new quantitative T1-mapping technique with potential in more clearly identifying myocardial inflammation and scar. SASHA and most SR methods use a 90-degree RF pulse after which a signal is recorded at a certain inversion time. This is repeated seven more times at increased inversion times across separate heartbeats to create a T1 curve. Saturation recovery is beneficial since it needs no correction for underestimated T1 values. The 90-degree pulse allows for a more direct estimate of T1 since the magnetization memory is erased from prior cycles. SASHA is known to have higher accuracy but lower precision. SASHA is also found to be more prone to noise artifact. Due to its lower precision, there is a lower reproducibility but consistent accuracy (

Figure 1).

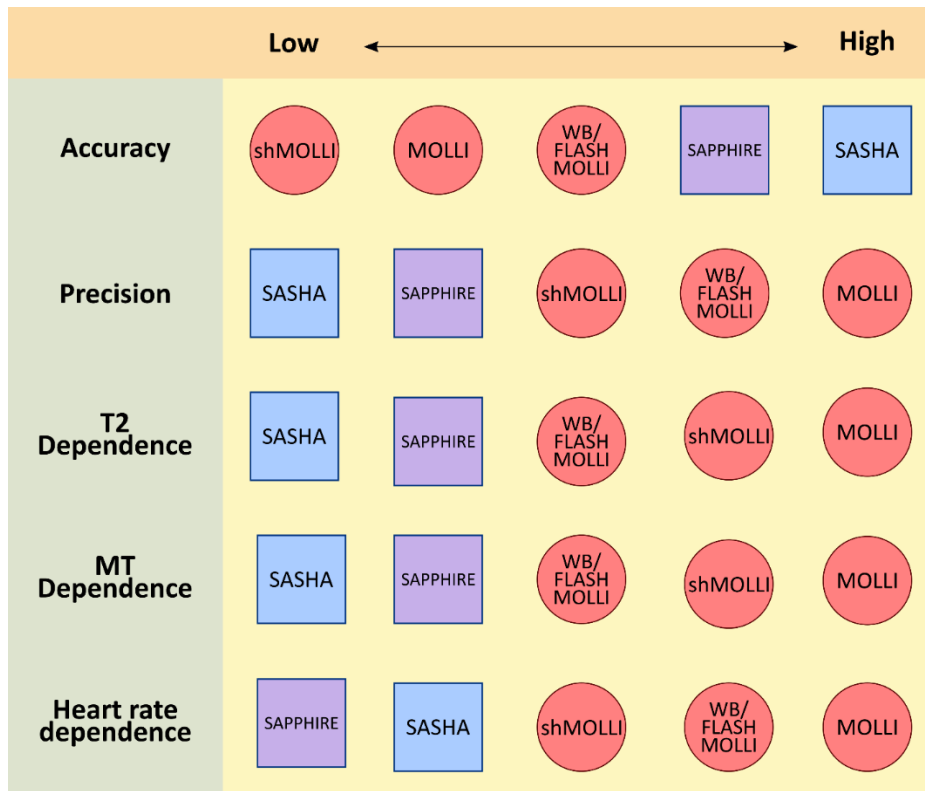


Figure 1. Comparison of T1-mapping sequences including MOLLI, shMOLLI, SASHA, and Saturation Pulse Prepared Heart-Rate Independent Inversion Recovery (SAPHIRE).

1.4 Gradient Echo Sequence Readouts

Images obtained using CMR have a variety of readout methods after collecting the data from the RF data. Inside the main magnet are three gradient coils which produce the magnetic field, B_0 . The gradient echo (GRE) is produced by using a single RF pulse in one direction and then reversed, resulting in an echo. By using one RF pulse, it reduces scan time compared to other basic pulse sequences, like spin echo, therefore forming the basis of most standard rapid MRI sequences. After the initial excitation, the resulting gradient begins to de-phase. When the reversal is applied, the gradient will begin to rephase. (1, 27).

Flip angles are defined as the angle in which the longitudinal vector is displaced from equilibrium. Large or small flip angles create large or small transverse magnetization, respectively. For rapid sequences, a smaller flip angle is desired as they are crucial in determining tissue contrast in GRE sequences (1). GRE imaging requires strong field homogeneities. It is important to note that GRE can only refocus spins that have also been rephased by that same gradient therefore more highly affected by field inhomogeneities that affect the phasing.

1.4.1 Balanced Steady-State Coherent Gradient Echo

One type of GRE sequence is the balanced steady-state free precession (bSSFP) coherent sequence. Balanced indicates that the net gradients are zero or are fully rephased before the next excitation pulse. Coherent GREs broadly imply that no transverse magnetization from the reversal gradient remains (28, 29). The signal intensity resulting from the coherent sequence comes to be a ratio of $T2/T1$. For solid tissues like muscle and fat, the ratio is low, 0.05 and 0.30, respectively. Fluids demonstrate a higher ratio upwards of 0.70 creating an excellent base for CMR imaging (28, 30, 31). The higher signal to noise ratio (SNR) provides good contrast in T1 images and potentially reducing noise from CIED artifact. Common trade names for this kind of sequence include: True FISP (TRUFI) (Siemens), FIESTA (GE), True SSFP (Toshiba), and Balanced FFE (Phillips). For consistency, the remainder of this report will be using Siemen's tradenames representing bSSFP.

1.4.2 Incoherent "Spoiled" Gradient Echo Sequence

In contrast, there is also an incoherent, "spoiled" gradient echo sequence. Compared to coherent sequences, incoherence deals with residual transverse magnetization that may be the result of small flip angles. The successive signals "spoiled" by including a phase shift as the receiver can

distinguish the phases from previous, successive RF pulses. As a result, T1-weighted images are generated with little to no T2 dependence with typically moderate to large flip angles.

Common trade names for this sequence include: FLASH (Siemens), MPGR (GE), and Field Echo (Toshiba). For consistency, an incoherent “spoiled” gradient echo will be referred to by Siemen’s tradename, FLASH.

1.5 Degradation in Diagnostic Image Quality Due to Implanted Cardiovascular

Electronic Devices in Cardiac Sarcoidosis Patients

The aim of medical imaging is to obtain diagnostic scans free of artifact and without substantial degradations in imaging. In CMR, it is especially important to be able to have high contrast images of the myocardium with adequate spatial resolution to visualize smaller details of the heart. Any potential distortions, small or large, may gravely affect the clinical value of the scan.

In recent years, the safety of patients with implanted devices have been taken into consideration for MRI. Devices are marketed as MR conditional, MR safe, and MR unsafe. While the latter option poses a hazard to the highly magnetic environment, the first two options can be safely scanned within the patient (32). Although they are marked as such, it does not mean that they will not induce off-resonant artifact onto the image from the magnetic field interacting with the ferrous metal of the device and its components. Patients with potential myocarditis and other diseases with high scar burden (and thus arrhythmogenic potential) may already have CIED in order to prevent arrhythmias and sudden cardiac death. With the device in mind, potential artifact from the devices can affect patient scans. Leads from devices like pacemakers can create voids in the atrium, ventricle, or both depending on the necessary placement. The generator box placement is a bit bulkier, typically placed subcutaneously below the left clavicle. This can introduce even larger

voids in CMR scans and off resonant artifact. One way to combat the artifact surrounding the heart is to physically move it. Technicians have the patient lift their arm above their head and keep it in place for the scan. This can potentially move the artifact away from the myocardium enough for diagnostic quality. In some cases, this may be sufficient but having the patient maintain this position can be laboring and introduce other complications to the process.

Another difficulty in CMR is the differentiation between focal and diffuse myocardial fibrosis. While focal fibrosis is concentrated and easily distinguished in LGE images, diffuse fibrosis is more difficult to detect as it is spread out and patchy. Diffuse fibrosis is prominent in patients diagnosed with CS (33). Patients with CS are typically recommended to have a CIED to assist with any resulting cardiac complications such as arrhythmias or sudden cardiac death. While WB LGE has shown promise in allowing diagnostic imaging of patients with focal fibrosis, diagnostic T1 mapping could potentially capture subclinical changes in pathology including inflammation and fibrosis.

In addition to artifact introduced by CIED, the difficulty in identifying diffuse scarring and inflammation becomes even more challenging. Native T1-mapping is non—specific to scar unless contrast is given. Combination of T1 and T2-quantitative mapping may improve diagnostic accuracy and identification of inflammation and scar (34). Cardiac sarcoidosis patients require a better way to identify diffuse scar and safely monitor the extent and progression of the disease. There is a disparity for imaging sarcoidosis patients with CIEDs. Imaging modalities like PET/CT require ionizing radiation while current CMR standard sequences are not fully capable of acquiring artifact-free images due to the challenging circumstances.

While certain MRI techniques like LGE and MOLLI have been well established and researched, saturation recovery methods like SASHA have yet to be fully explored. SASHA may have the potential to overcome CIED artifact in cardiac sarcoidosis patients while preserving or enhancing image quality for diffuse scar in the myocardium.

1.6 Specific Aims and Objectives

The specific objectives of this research are to confidently measure T1 values by comparing myocardial images of cardiac sarcoidosis patients with implanted devices taken with different sequences (MOLLI and SASHA) and readouts (FLASH and TRUFI) resulting in four separate T1 mapping sequence combinations.

Aim 1: Determine image quality of scans using MOLLI and SASHA protocols with varying readouts, TRUFI and FLASH, in patients with sarcoidosis and CIEDs using a 5-point scale: 5 (excellent), 4 (good), 3 (fair), 2 (poor), and 1 (non-diagnostic).

Hypothesis 1: SASHA with a FLASH readout will have higher image quality scores due to less susceptibility to off-resonant artifacts from CIEDs.

Aim 2: Determine the variance and reproducibility between quantitative T1 mapping sequences MOLLI and SASHA with varying readouts, TRUFI and FLASH, in cardiac sarcoidosis patients with devices.

Hypothesis 2: The SASHA method with a FLASH readout will show little to no discrepancy between initial and secondary exams due to those methods being less susceptible to field inhomogeneity.

High overall image quality score with reproducible quantification will indicate which imaging protocol is best suited to scan patients with CIED artifact for diagnostic value.

2 Quantitative T1-Mapping and Analysis

2.1 Rationale and Hypotheses

Current imaging modalities and methods are not properly addressing the needs of patients with sarcoidosis and CIEDs. Modalities like PET/CT, x-ray, and fluoroscopy all use low dosage ionizing radiation. Although not immediately a danger, constant exposure may pose adverse health effects. LGE and WB-LGE have shown to be useful in imaging focal scarring but not diffuse scar in patients with cardiac sarcoidosis and implanted devices. On top of well-recorded device artifact, LGE particularly does poorly in distinguishing diffuse scar due to needing a myocardial reference to find the difference between signal intensity. Diffuse fibrosis does not have well defined edges for effective detection. Widely used inversion recovery methods like MOLLI also have three key issues. First, MOLLI has shown to have a T2 dependence. Studies have shown phantoms with shorter T2, in the 46ms to 76ms range, greatly underestimate T1 values. This trend is seen in-vivo with even greater underestimation. In simulation, underestimations were also inconsistent. Second, MOLLI has also shown high dependence on magnetization transfer as signals from the free pool protons are mixed with the intracellular bound pool. Due to the summation of Look-Locker sequences in MOLLI, the effect of MT for each image is compounded and cumulatively contributes to underestimations of T1 values. Finally, MOLLI has shown to have imperfect inversion efficiency. One study suggests a correction of $14.0 \pm 6.6\%$ to estimate a true T1 from conventional MOLLI sequences following trends determined from other tissue (35).

While certain MRI techniques like LGE and MOLLI have been well-established and researched, saturation recovery methods like SASHA have yet to be fully explored. SASHA may have the

potential to overcome CIED artifact in cardiac sarcoidosis patients while preserving or enhancing image quality for diffuse scar in the myocardium.

2.2 Methods

2.2.1 Study Design

This study is a sub-analysis for the Feasibility Phase of Cardiac Sarcoidosis Multi-Center Randomized Controlled Trial to quantitatively determine myocardial inflammation and scar in cardiac sarcoidosis patients with implanted cardiac devices. Five patients with clinically active sarcoidosis were recruited from the VCU Sarcoidosis Clinic. Interpreters were blinded and randomized to ensure equal distribution of devices across studies. Inclusion criteria were based on CS Heart Rhythm Society Diagnostic Criteria (36). This involved patients with one or more of the following clinical findings: histological diagnosis from myocardial tissue, clinical diagnosis from invasive and noninvasive studies, and no alternative explanation for clinical features. Patients with implanted devices must be at least 6 weeks post-implantation. Exclusion criteria were as follows: patient unwilling or unable to provide informed consent, patient has a contraindication to CMR or severe claustrophobia, renal disease with creatinine $> 1.5\text{mg/dL}$, pregnancy, or breastfeeding. All patients enrolled in the program provided written and witnessed informed consent following Institutional Review Board of Virginia Commonwealth University approval. Scans consist of global values and axial slice-based values for the basal, mid-cavity, and apical slices of the left ventricle. Each slice was further segmented into 6 regions for segmental analysis.

Study participants were asked to come into the clinic to be scanned using the four combinational sequences. They were then asked to be rescanned within two weeks after the initial scan.

2.2.2 CMR Protocol

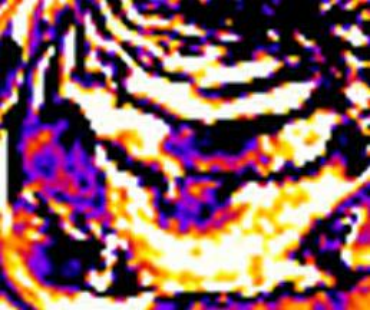
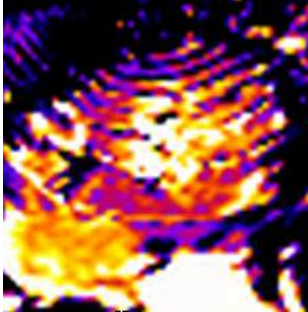
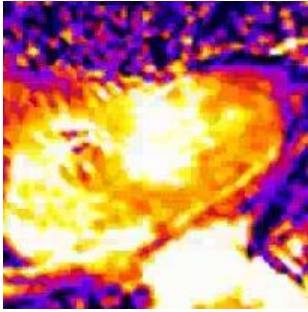
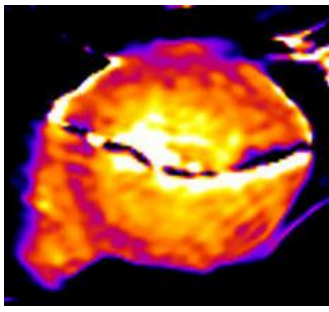
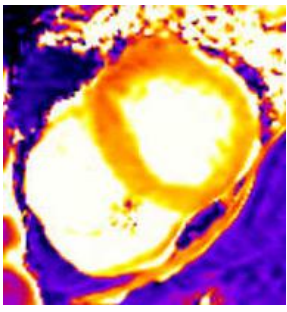
All five participants in this study underwent CMR imaging on a 1.5T Siemens Magnetom Aera scanner (Malvern, PA). Participants' left arm was placed above their head in order to physically move the generator box – a technique done to minimize interfering CIED artifact in the myocardial region. The Siemens' Quantitative Cardiac Parameter Mapping (T1, T2, T2*, ECV) work in progress (WIP) #1041B (VE11C) was used for mapping sequences. For consistency, the remainder of this report will reference Siemens' tradenames for all readouts. After localization of the heart, the protocol applied four different T1 mapping sequences pre-contrast: A MOLLI 5(3)3 sequence (which refers to 5 acquisition heartbeat, followed by 3 recovery heart beats, followed by 3 more acquisitions) and 2-parameter SASHA sequence were used with varying readouts FLASH and TRUFI with a 35-degree flip angle and 8mm slice thickness or 70-degree flip angle and 8mm slice thickness, respectively. The FLASH readout sequence was added to the imaging protocol partway into the study due to ongoing updates. Images were taken at the base, mid-cavity, and apical short-axis positions of the heart using a 5-slice reference scout to ensure matched tissue characterization localization between study visits. T2 maps were then recorded involving 3 T2 preparations at 0, 25, and 55ms with recovery periods of 4 seconds with varying readouts FLASH and TRUFI at the base, mid-cavity, and apical slices with a 35-degree flip angle and 8mm slice thickness or a 70-degree flip angle and 8mm slice thickness, respectively. Participants were then injected with contrast (0.15 mmol/kg gadopentetate dimeglumine) and imaged again with a MOLLI 4(1)3(1)2 scheme and a 2-parameter fit SASHA with participants at a heart rate of 90 bpm or greater in the same 3 slices as native T1 maps. Patients returned to the hospital for a repeat scan following the same procedure after X weeks.

2.3 Qualitative Analysis

The endocardial and epicardial analysis were done by the one researcher which were verified by the principal investigator. Image segments were given an image quality score (IQS) from a pre-defined scale ranging from 1 (non-diagnostic), 2 (poor), 3 (fair), 4 (good), 5 (excellent) (37). Six segments of each region, basal, mid-cavity, and apical, were graded according to the scale by a single investigator.

This scale is sourced from previous studies by Kellan et al for uniform extracellular volume fraction (ECV) maps. **Table 1** contains the visual descriptions and written criteria for each IQS (37).

Table 1. Visual and written criteria for image quality scoring for quantitative T1-values.

Non-diagnostic	Poor	Fair	Good	Excellent
				
<p>T1 values could not be measured reliably anywhere in the myocardium.</p>	<p>Inhomogeneities or geometric distortion affected greater than 50% of the myocardium.</p>	<p>Criteria under the excellent category were absent, or geometric distortion was present, or multiple regions had inhomogeneity deemed to be artifactual but affected less than 50% of the myocardium.</p>	<p>One of the criteria under excellent was absent, or geometric distortion were present but not impacting the T1 values, or there were small regions (10%) of inhomogeneity in the myocardium.</p>	<p>Myocardial borders were crisp and distinct from the blood pool with less than or equal to 1 pixel of partial volume border and no noticeable geometric distortion.</p>

2.4 Quantitative Analysis

Quantitative analysis was done using commercially available software cvi42 by Circle Cardiovascular Imaging (Calgary, AB). Epicardial and endocardial contours were manually drawn and then verified by a second party with a 10% contour offset to ensure that the blood pool and epicardial fat were excluded from the contours. Each slice of the myocardium was segmented into 6 regions following major coronary artery territories based on the American Heart Association (AHA) 17-segment model (38). All T1 averages and standard deviations per region were automatically calculated within the software and exported for statistical analyses.

2.5 Statistical Analysis

Statistical analyses were performed in MATLAB using their statistical toolkits and built-in functions. Slices or segments deemed non-diagnostic were excluded from the statistical analysis.

A paired t-test was applied between patients' T1-values from their initial and secondary visits to determine any scan-to-scan variation at a 95% confidence level.

An analysis of variance (ANOVA) test was conducted on the T1 values between SASHA and MOLLI scans and then all four methods: SASHA TRUFI, SASHA FLASH, MOLLI TRUFI, and MOLLI FLASH. The significant p-value was recorded at a 95% confidence level. An ANOVA test was used to determine if the variance in means of the data was statistically significant.

A Tukey-Kramer post hoc test was performed on statistically significant results from the ANOVA to determine a statistically significant pairs within the group. Finally, a coefficient of variation (CoV) measurement was done between T1 values to determine relative dispersion.

Due to the natural difference in inversion recovery and saturation recovery methods where the former leads to underestimation and lower T1 values, the delta of the data was analyzed when appropriate.

2.6 Results

Participants were mainly middle-aged women with an average of 35.4 months since CS diagnosis. The time range between CMR examinations were extended due to SARS-CoV-2 pandemic restricting patient travel and clinical operation (**Table 2**). Out of five patients, one patient's scan was severely impacted by artifact and was not included in the analysis (**Figure 2**).

Table 2. Patient demographic and characteristics.

Clinical Characteristics	N
Women, n (%)	4 (80%)
Race, n (%)	
Black	3 (60%)
Caucasian	2 (40%)
Mean age, years	41 (range 38-61)
Time since CS diagnosis, months	35.4 (range 38-53 months)
Time between CMR examinations, days	19.25 (range 1-64 days)
Device type, n (%)	
Boston Scientific	3 (60%)
Medtronic	2 (40%)

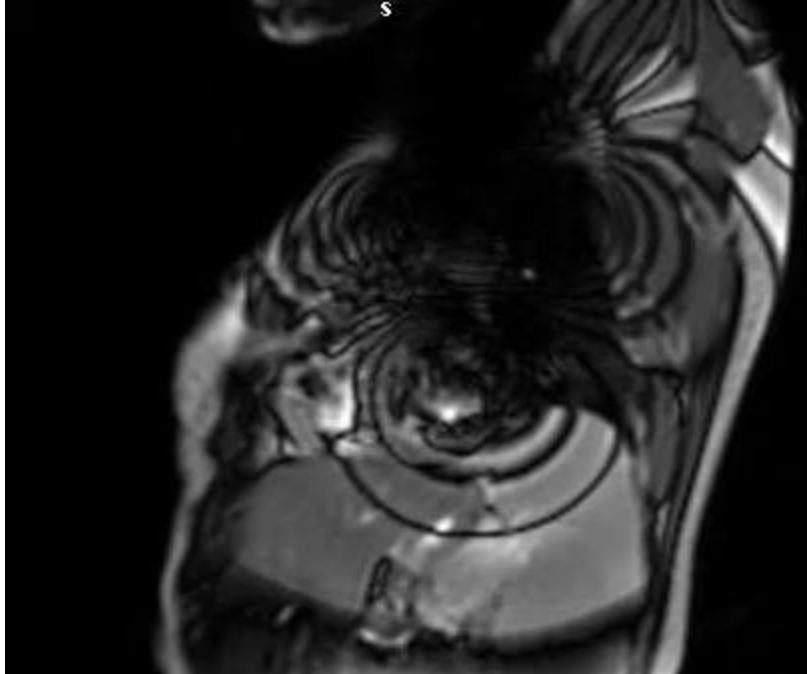


Figure 2. Localizer scan with severe artifact for participant two. As a result, participant two was not included in analysis.

2.6.1 Determination of Image Quality Between Methods

Image quality scores from each segment of scans were tabulated in and used to calculate an average for the entire region. In a slice-based analysis, 92.86% of regions scanned with SASHA were scored above a poor rating while 83.33% of regions scanned with MOLLI were scored fair or better (**Figure 3, Figure 4**).

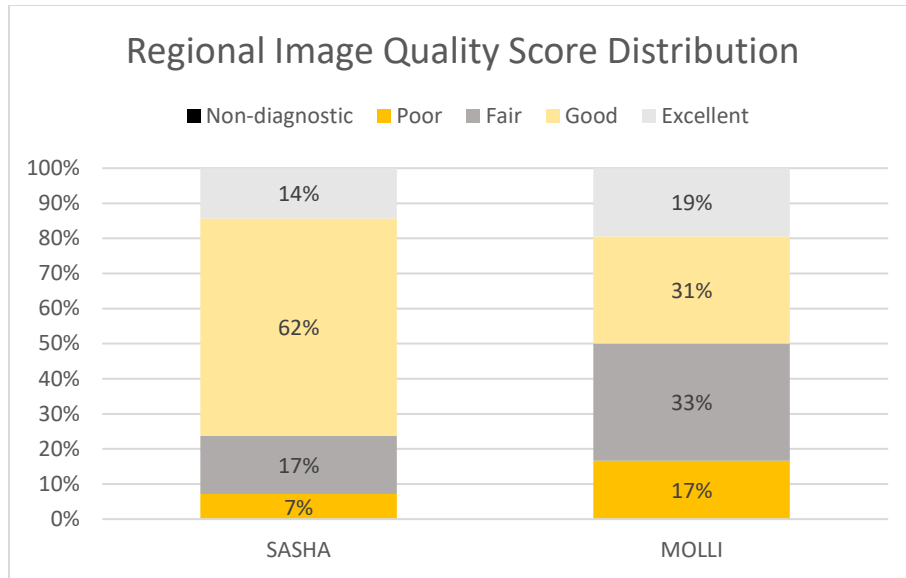


Figure 3. Image quality score distribution between SASHA and MOLLI scans of the heart. Slice-based scores were averaged from segmental scoring in pre-contrast scans.

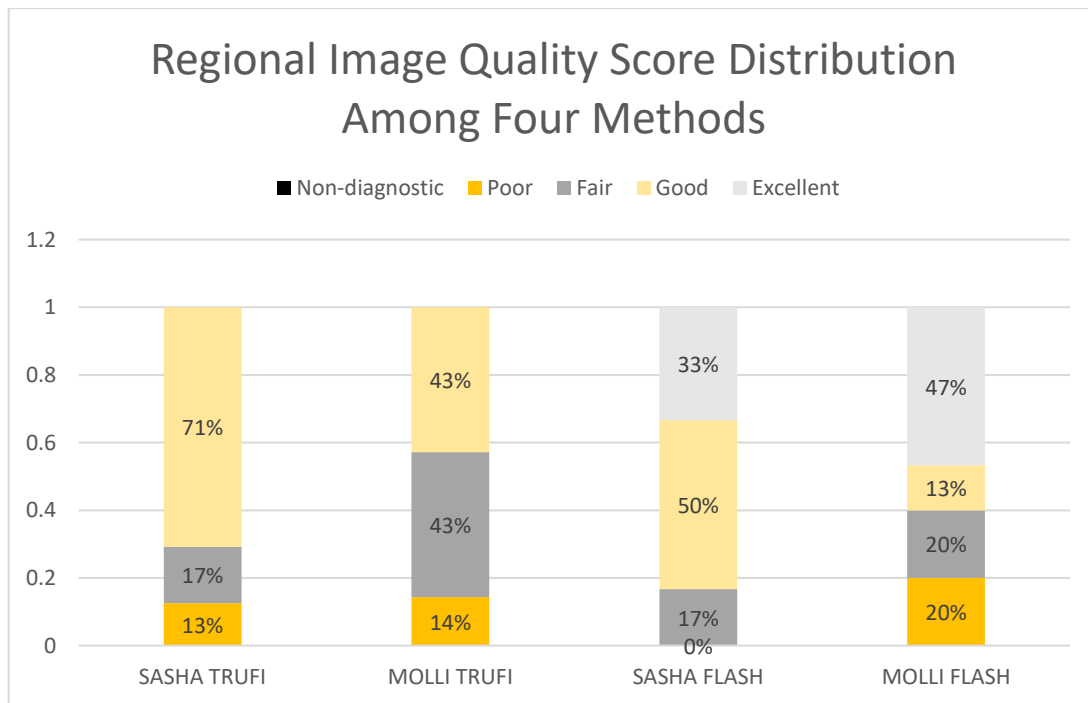


Figure 4. Distribution of slice-based image quality scores among the four methods: SASHA TRUFI, MOLLI TRUFI, SASHA FLASH, and MOLLI FLASH in pre-contrast scans.

Furthermore, within SASHA, 87.50% of regions (n=24) with a TRUFI readout were deemed fair or better while 100% of regions (n=18) with a FLASH readout were evaluated to be fair or better.

Within MOLLI scans, 85.71% of regions (n=21) with a TRUFI readout were scored fair or better with 0% of regions being excellent. 80.00% of FLASH slice-based readouts (n=15) with MOLLI were scored above a poor rating.

2.6.2 Analysis of Native T1-Values

As shown in **Table 3**, MOLLI T1-values were generally lower than SASHA T1-values. Values are given for the entire scan and then for each slice.

Table 3. Global and slice-based coefficient of variance and T1-values (ms) for all participants for the basal (B), mid-cavity (M), and apical (A) slices.

		SASHA				MOLLI			
		Global	B	M	A	Global	B	M	A
TRUFI	Visit 1	0.24 (1245 ± 299)	0.27 (1257 ± 339)	0.20 (1202 ± 238)	0.23 (1277 ± 296)	0.37 (695 ± 259)	0.21 (654 ± 269)	0.17 (592 ± 202)	0.16 (879 ± 210)
	Visit 2	0.22 (1251 ± 273)	0.13 (1198 ± 158)	0.23 (1240 ± 291)	0.25 (1328 ± 334)	0.29 (859 ± 252)	0.37 (801 ± 293)	0.29 (851 ± 249)	0.15 (950 ± 144)
FLASH	Visit 1	-	-	-	-	-	-	-	-
	Visit 2	-	-	-	-	-	-	-	-
TRUFI	Visit 1	0.45 (1094 ± 491)	0.36 (1222 ± 442)	0.48 (1098 ± 529)	0.51 (886 ± 449)	0.37 (515 ± 340)	0.48 (687 ± 332)	0.73 (464 ± 339)	0.69 (355 ± 246)
	Visit 2	0.29 (1179 ± 339)	0.29 (1189 ± 340)	0.23 (1137 ± 261)	0.35 (1234 ± 436)	0.63 (619 ± 388)	0.64 (609 ± 388)	0.66 (634 ± 419)	0.54 (618 ± 331)
FLASH	Visit 1	0.27 (1157 ± 317)	0.28 (1159 ± 322)	0.25 (1239 ± 313)	0.30 (1115 ± 330)	0.58 (792 ± 457)	0.46 (965 ± 442)	0.62 (709 ± 437)	0.65 (663 ± 432)
	Visit 2	1157 ± 276	0.27 (1166 ± 321)	0.24 (1296 ± 249)	0.16 (1146 ± 189)	-	-	-	-
TRUFI	Visit 1	0.29 (1245 ± 363)	0.17 (1228 ± 213)	0.21 (1213 ± 281)	0.41 (1291 ± 527)	-	-	-	-
	Visit 2	0.28 (1168 ± 324)	0.24 (1220 ± 292)	0.36 (1117 ± 398)	0.20 (1164 ± 234)	0.28 (829 ± 236)	0.25 (943 ± 236)	0.20 (804 ± 159)	0.34 (708 ± 237)
FLASH	Visit 1	0.29 (1251 ± 363)	0.18 (1234 ± 225)	0.21 (1217 ± 252)	0.41 (1304 ± 537)	0.50 (720 ± 356)	0.35 (697 ± 245)	0.43 (674 ± 288)	0.64 (806 ± 515)
	Visit 2	0.11 (1137 ± 131)	0.13 (1143 ± 151)	0.11 (1140 ± 85)	0.09 (1127 ± 103)	0.19 (836 ± 156)	0.19 (858 ± 165)	0.21 (815 ± 173)	0.12 (833 ± 100)
TRUFI	Visit 1	0.22 (1188 ± 257)	0.86 (1182 ± 169)	0.68 (1168 ± 797)	0.40 (1230 ± 496)	0.24 (880 ± 208)	0.23 (880 ± 198)	0.29 (879 ± 252)	0.14 (885 ± 121)
	Visit 2	0.30 (1172 ± 346)	0.30 (1229 ± 370)	0.33 (1165 ± 73)	0.14 (1075 ± 150)	0.16 (918 ± 151)	0.18 (921 ± 170)	0.16 (897 ± 157)	0.12 (944 ± 112)
FLASH	Visit 1	0.13 (1184 ± 156)	0.90 (1161 ± 174)	0.77 (1157 ± 95)	0.48 (1260 ± 101)	0.13 (882 ± 115)	0.13 (900 ± 121)	0.14 (867 ± 118)	0.10 (869 ± 87)
	Visit 2	0.09 (1177 ± 104)	0.09 (1177 ± 106)	0.08 (1153 ± 88)	0.09 (1211 ± 113)	0.10 (876 ± 84)	0.11 (860 ± 99)	0.08 (883 ± 71)	0.07 (895 ± 64)

In comparison of slice-based values, MOLLI TRUFI showed significant difference in means between initial (654 ± 269 ms) and secondary (801 ± 293 ms) visits (p -value=0.024) from a paired t-test while other methods did not show a significant change.

In a comparison of global values, there were no recorded statistically significant difference in initial and secondary scans (

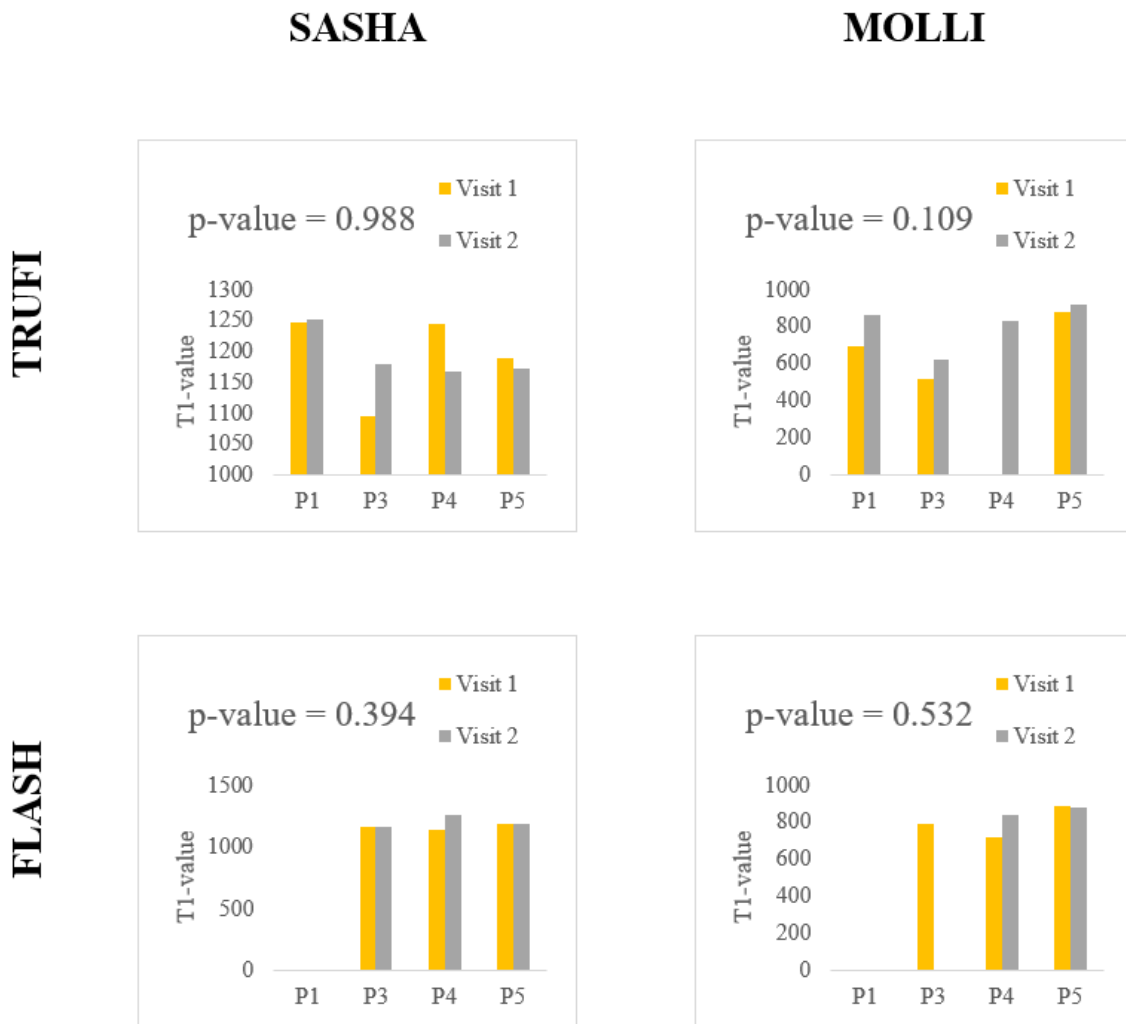


Figure 5).

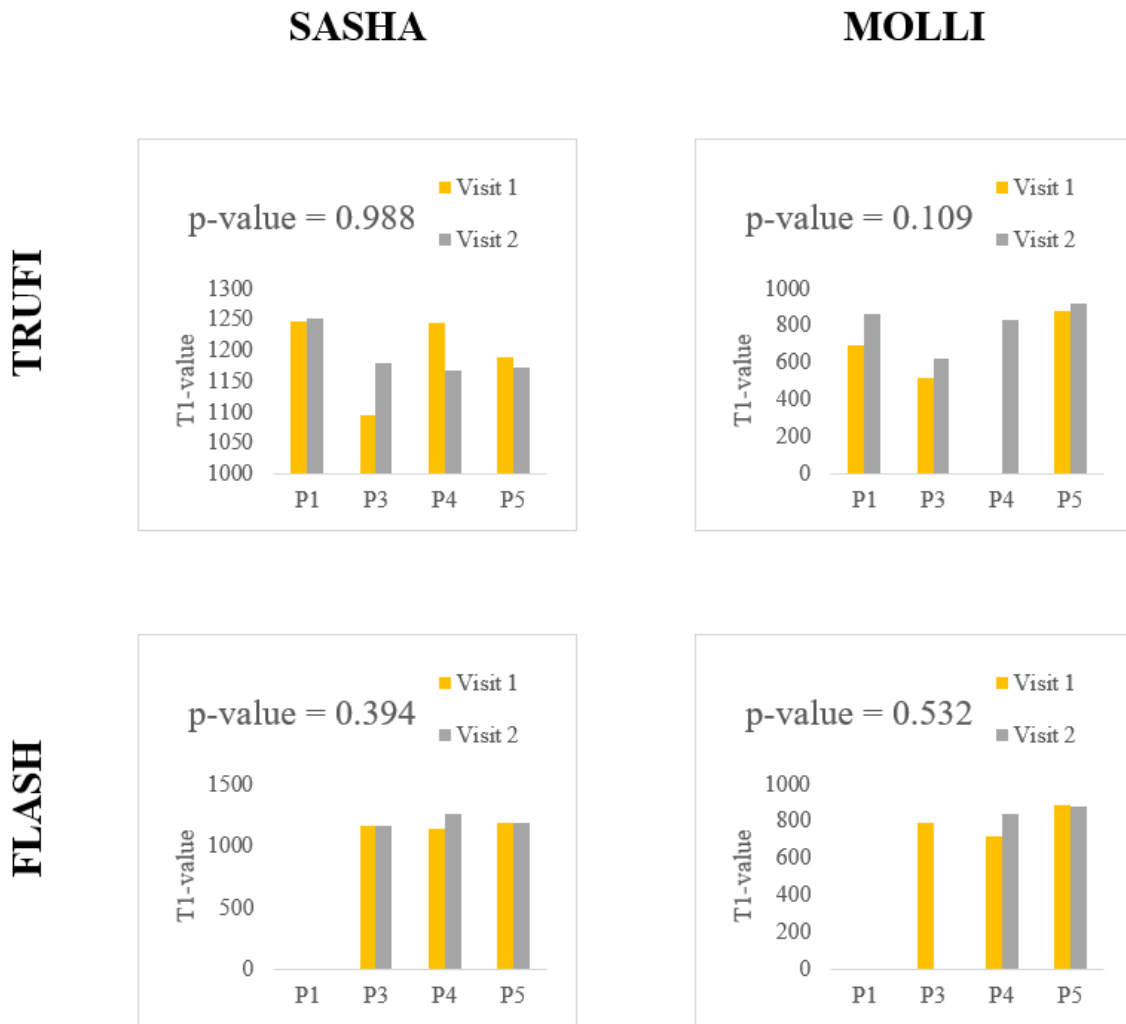


Figure 5. Comparison of global initial and secondary T1-values across the four methods. Student's t-test p-value result is reported.

Under an ANOVA test, global delta values for MOLLI and SASHA scans again did not suggest a significant variance in the means of their respective data with a sample size of four. As there was no significance, no post-host analysis was performed (**Figure 6**).

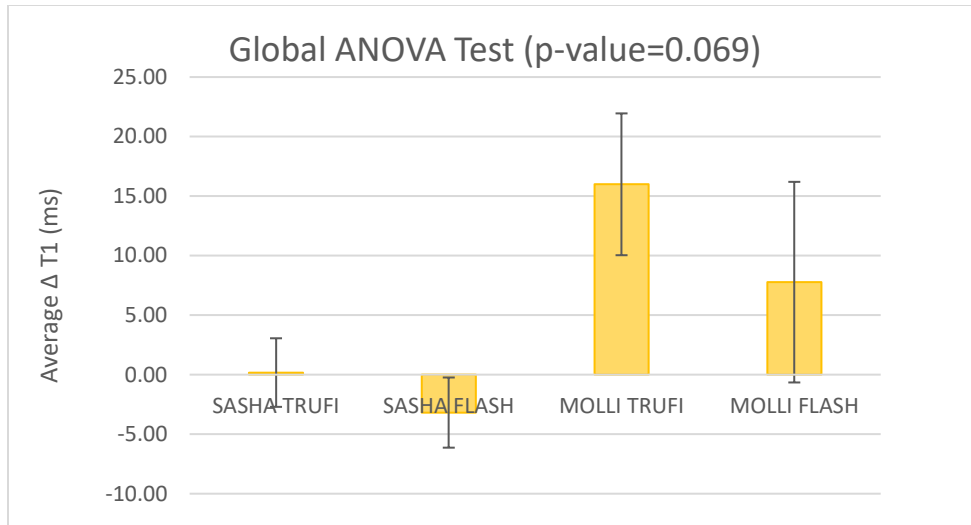


Figure 6. Graphical representation of global ANOVA test done between SASHA TRUFI, SASHA FLASH, MOLLI TRUFI, and MOLLI FLASH in pre-contrast scans.

Further analyses of slice-based T1 values suggest there are significant differences among the four methods with a p-value=0.0184. A Tukey-Kramer post-hoc test was performed and determined that SASHA TRUFI + MOLLI TRUFI and SASHA FLASH + MOLLI TRUFI exceeded the critical value (q_{crit}) of 3.83 with 32 degrees of freedom (df) (**Figure 7, Figure 8**).

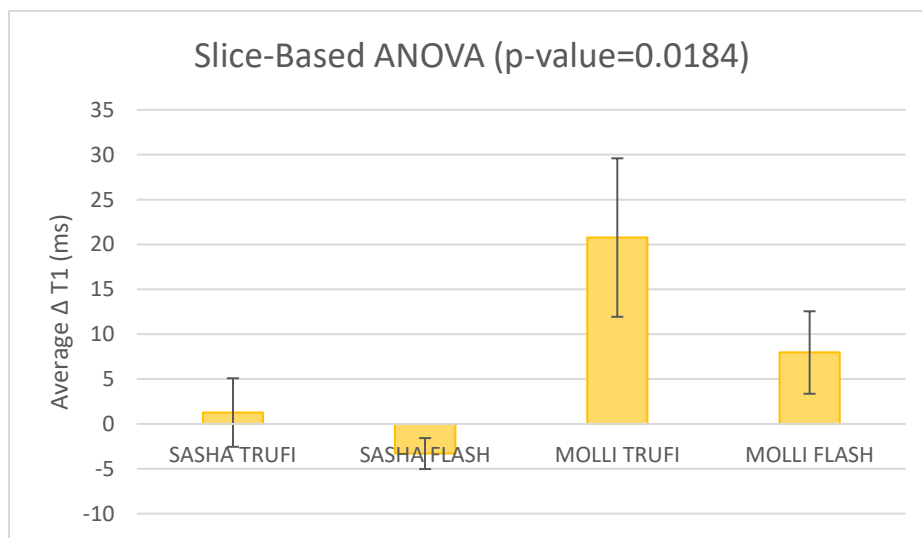


Figure 7. Graphical representation of slice-based ANOVA results between SASHA TRUFI, SASHA FLASH, MOLLI TRUFI, and MOLLI FLASH in pre-contrast scans.

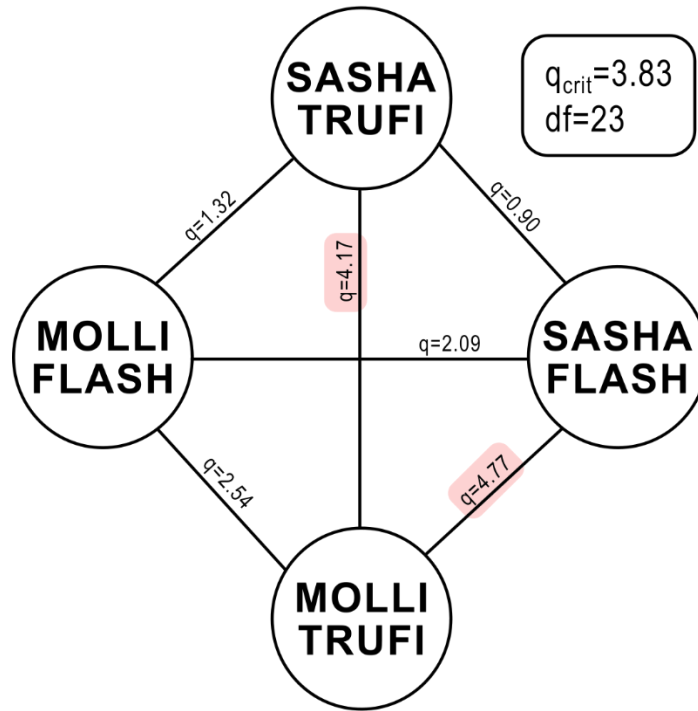


Figure 8. Tukey-Kramer results showing variations between the four methods and their q-values for native T1-values.

MOLLI CoV overall showed higher variability in relation to the average T1 values when compared to SASHA methods in global T1 values. Under slice-based analysis, SASHA methods tend to have a higher CoV specifically in the apical slices while MOLLI favored the basal and mid-cavity. Global and slice-based TRUFI readouts had a higher variation compared to FLASH. Overall MOLLI FLASH had the lowest CoV (Table 3).

2.7 Discussion

In

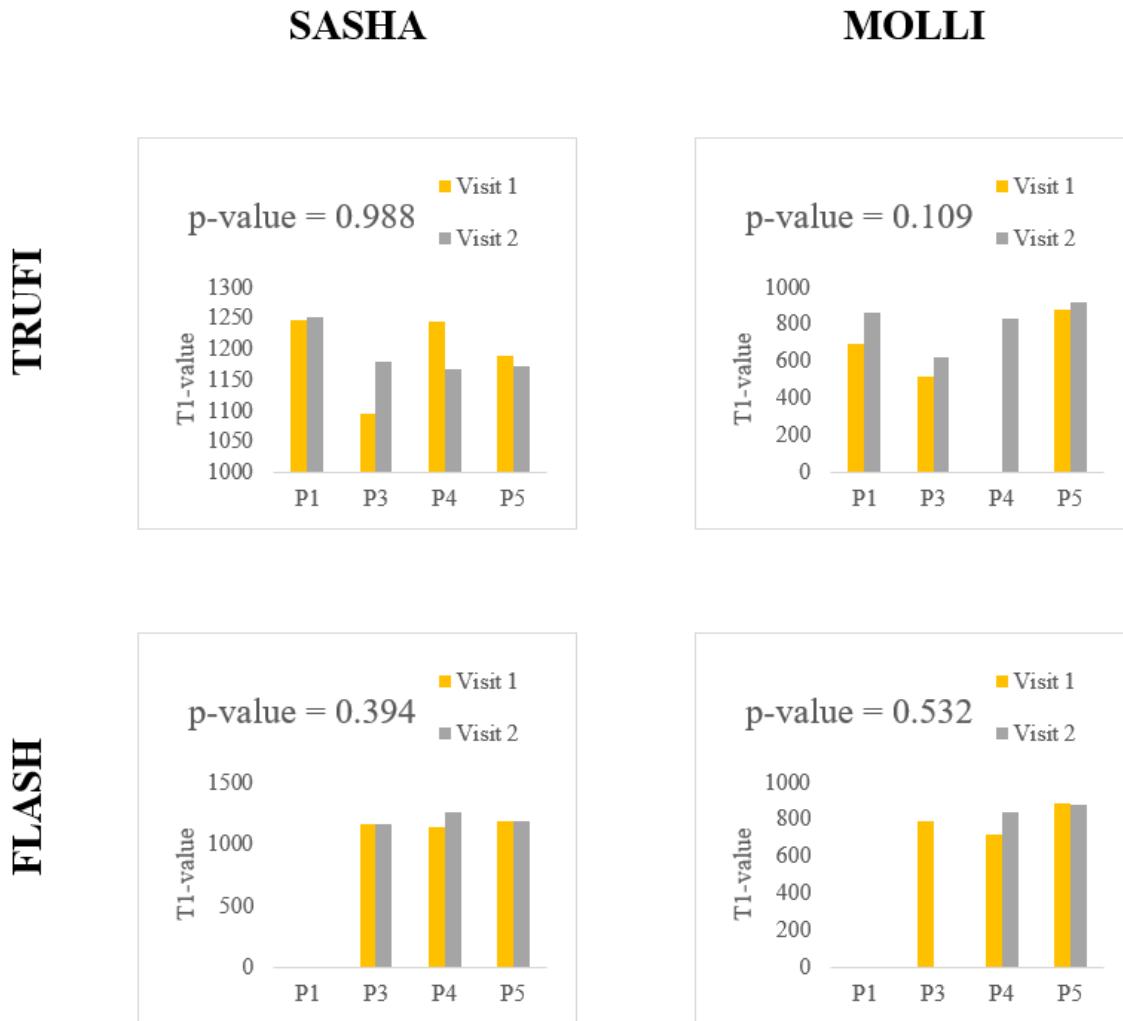


Figure 5 there are no significant differences in initial and secondary visits. Deeper analysis of slice-based values suggest MOLLI TRUFI may not be as reproducible as the other three methods (**Figure 7**). This result does not agree with current literature that suggests MOLLI tends to have higher reproducibility when done in a head-to-head comparison of MOLLI, SASHA, and other quantitative methods in phantom scans with global values (39). While previous studies were done

in phantom studies and healthy volunteers, MOLLI TRUFI has shown to underperform in CS patients with devices against SASHA variants and MOLLI FLASH.

By scrutinizing slice-based results, MOLLI TRUFI may not offer the best reproducibility for diagnostic purposes when looking at specific regions like the basal or mid-cavity slices. Results of an ANOVA test done on slice-based values called for a Tukey-Kramer test to identify the specific cause for significant difference in means (**Figure 7**). A post hoc analysis was done on every combinational pair of methods. Pairs with MOLLI TRUFI exceeded in q_{crit} and suggesting a significant difference. This may suggest that MOLLI with a TRUFI readout may be the least reliable in terms of repeatability whereas all other pairs did not show any significant difference. From these results, MOLLI may not be preferred compared to other methods like SASHA for monitoring disease progression or continual impact in patients as values may vary from scan to scan between longer periods of time. While there is limited study on how readout may affect the variance and reproducibility of a scan, FLASH may be preferred for consistent scanning.

Between initial and secondary visits, MOLLI demonstrated significant differences in both FLASH and TRUFI readouts compared to SASHA on a slice-based level (**Figure 7**). As a result, MOLLI may have higher variability and not be as reproducible in patients with devices as previous literature has only been done in healthy participants (40). One study has found the native T1 test-retest variability were higher in MOLLI compared to other inversion recovery methods (41). In addition. Another study finds that MOLLI may have underlying variability in slice-based T1 mapping which may call for further insight when done on eighteen healthy volunteers and no devices (42).

2.8 Limitations

The following limitations in this study must be taken into consideration when interpreting these results. First, this study was limited to a single clinic and single scanner. Results may vary between scanners and clinics when used with the protocols developed in this study. Second, the study had only five participants. One participant's scans were excluded from further analysis due to severe artifact effectively bringing the sample size to four. Although this was not a statistically powered study, the small number of participants must be taken into consideration to frame the results for further clinical use. Finally, amid the SARS-COV-2 pandemic, participants were not able to be retested within the two-week time frame. Although one participant was scanned 64 days later, it was determined that their condition had not changed significantly and would not affect the test-retest scan in that regard.

2.9 Conclusion

The first aim of this thesis was to qualify which of the four scanning methods produced the best image quality according to a pre-determined scale. The scale, which was previously used for evaluating ECV quality, was modified to work with T1 values. Between the two sequences, SASHA and MOLLI, SASHA had a higher percentage of scans deemed "fair". MOLLI is well documented to be dependent on MT, T2, and heart rate. These factors may have affected the slice-based results. MOLLI on the other hand outnumbered SASHA in every other category including scans deemed "poor" (**Figure 3**) on a global scale. SASHA may produce less non-diagnostic or "poor" scans with the trade-off of producing more "fair" rated regions. Taking a more in-depth look at how readout method may affect IQS, the same general trends followed. It is important to note that no TRUFI readout resulted in an excellent rating. From this, FLASH readouts coupled

with a SASHA sequence may provide a higher percentage of scans for diagnostic use (**Figure 3, Figure 4**).

Further, we wished to determine and quantify the reproducibility and variance of each method. While initial global analysis did not provide any indication which method may have significant differences between scans, slice-based analysis suggests MOLLI with a TRUFI readout (the most commonly utilized T1 mapping variant of the four compared) may not be the most reproducible. While this is not supported by current literature, further research is warranted to further justify the use of MOLLI or a TRUFI readout in patients with sarcoidosis and devices compared to other method and readout combinations. It is important to note the small sample size in this study as results may change with increased participation. As for the variance between scans a TRUFI readout may lead to more variability between scans (Figure 8). Using a post-hoc Tukey-Kramer test revealed that MOLLI TRUFI had a notable variance and did not agree well with the other methods. Regardless of sequence, the TRUFI readout may not be suitable for consistent use from scan to scan.

3 Ancillary Analysis

Further quantitative analysis can be done with T1 post-contrast values, segmental considerations, and T2 values. Post contrast values generally allow for higher visual and quantitative contrast between healthy and damaged myocardium. In addition, with T2 analysis, clinicians may better define inflammation and scar. A recent study suggests that at least one T1-marker and T2-marker are needed to increase specificity in identifying myocardial inflammation (34). While general practice takes images of the heart at three regions, further segmental analysis is useful in isolating areas of the heart from artifact that may be useful in analysis.

3.1 Post Contrast T1 Considerations

Following pre-contrast scans, participants were then injected with contrast and imaged again with a MOLLI 4(1)3(1)2 scheme and a 2-parameter fit SASHA with TRUFI and FLASH readouts. Evaluations of IQS and reproducibility of post-contrast scans were also performed.

SASHA and MOLLI scans were similar in IQS, although 3.03% of SASHA scanned regions were deemed excellent (**Figure 9**).

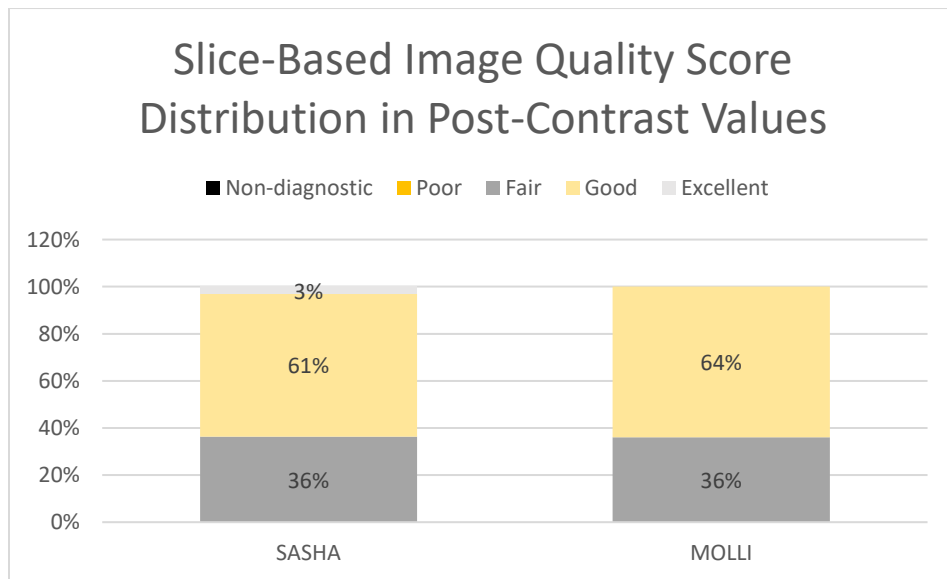


Figure 9. Image quality score distribution between SASHA and MOLLI scans of the heart. Slice-based scores were averaged from segmental scoring in post-contrast scans.

When comparing the four methods separately, MOLLI FLASH and MOLLI TRUFI generally outperformed the SASHA variants in the fair and good categories although only SASHA TRUFI contained any excellent ratings at 4.17% of all SASHA TRUFI scans (n=24) (**Figure 10**).

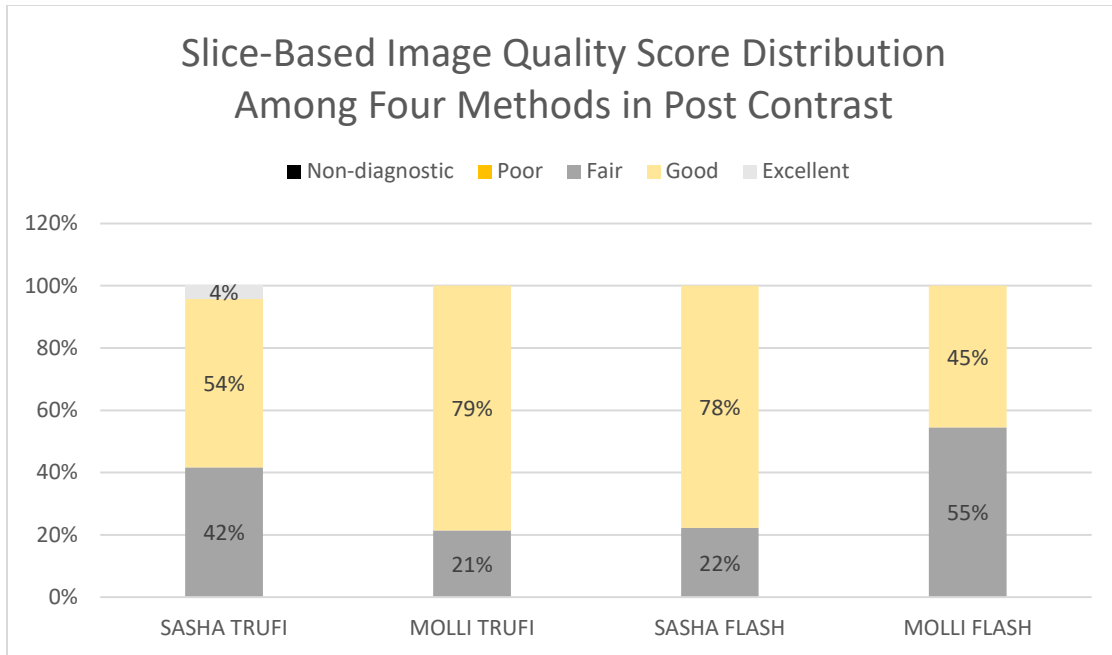


Figure 10. Distribution of slice-based image quality scores among the four methods: SASHA TRUFI, MOLLI TRUFI, SASHA FLASH, and MOLLI FLASH in post-contrast scans.

There was no significant difference between global values in initial and secondary visits under a paired t-test. Due to insufficient data, the SASHA FLASH method was not included. On average, slice-based SASHA TRUFI T1-values showed significant difference between initial (491 ± 264 ms) and secondary (530 ± 145 ms) visits (p -value=0.010). Under a one factor ANOVA test, global values between the four methods shown no significant difference in post-contrast means (p -value=0.815).

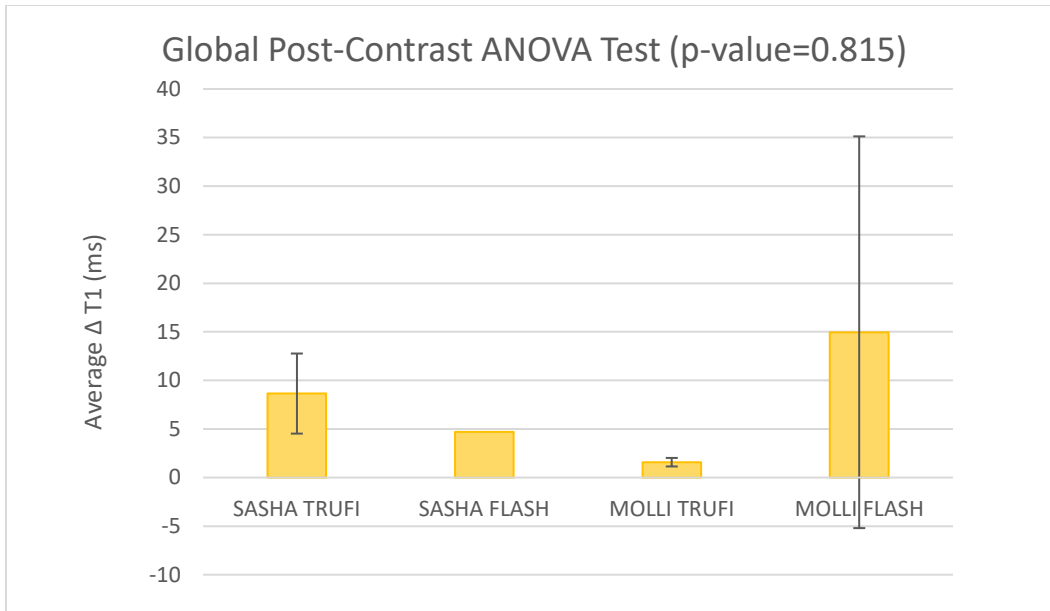


Figure 11. Graphical representation of global ANOVA test done between SASHA TRUFI, SASHA FLASH, MOLLI TRUFI, and MOLLI FLASH in post-contrast scans.

When considering the slice-based values, there was a significant difference in means between groups (p-value=0.012) with a 95% confidence (**Figure 12**). Further post hoc analysis showed that SASHA TRUFI+MOLLI TRUFI and MOLLI TRUFI+MOLLI FLASH have significant difference (qcrit=3.91, df=23) (Figure 13).

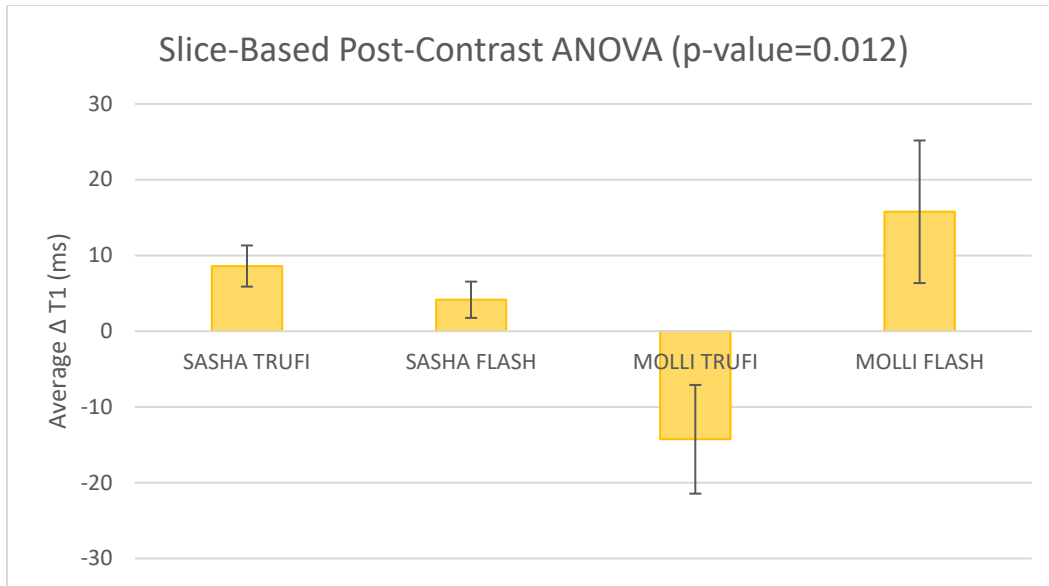


Figure 12. Graphical representation of slice-based ANOVA results between SASHA TRUFI, SASHA FLASH, MOLLI TRUFI, and MOLLI FLASH in post-contrast scans.

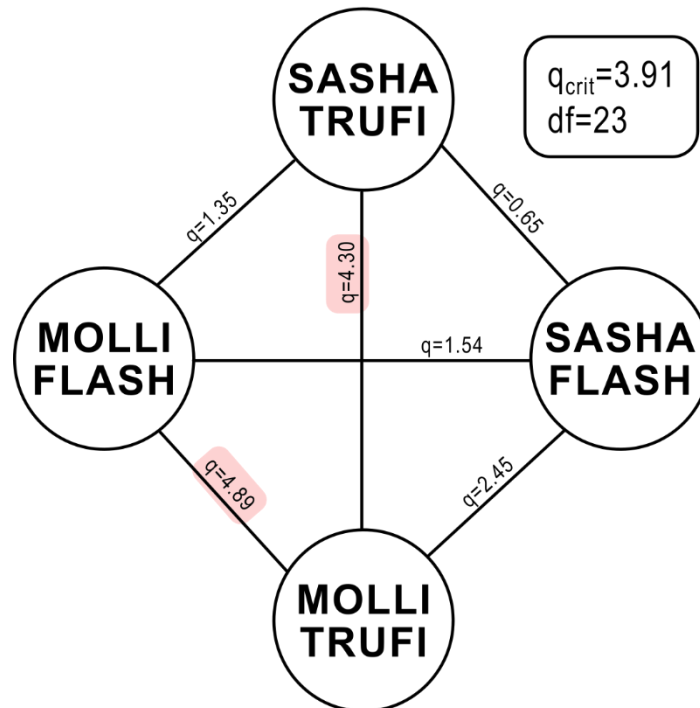


Figure 13. Tukey-Kramer results showing variations between the four methods and their q-values for post-contrast T1-values.

Looking at the CoV, 58.71% of post-contrast scans had higher variability globally when scanned with MOLLI. Slice-based, 63.89% of scans with SASHA showed a higher CoV indicating higher variability. Although not apparent when observing global values, looking at each slice shows that SASHA has more variability post contrast. The contrast, which shortens T1, may amplify SASHA's well documented imprecision (39, 43).

3.2 Segmental Considerations

Each short-axis slice can be split into six segments for analysis according to the AHA 17-segment model (38). In some cases, artifact may not be completely removed but some segment of the heart may still be viable for diagnostic purposes, thus an exploratory analysis using segmental values rather than slice-based or global values was performed.

In all SASHA scans, 98.81% of segments (n=252) were deemed diagnostic. 88.89% of segments (n=216) among all MOLLI scans were deemed diagnostic (**Figure 14**). In SASHA scans, 98.61% of segments (n=144) with TRUFI readouts were deemed diagnostic while 99.07% of segments (n=108) with FLASH readouts had diagnostic value. In addition, 88.23% of MOLLI segments (n=130) with TRUFI readouts were deemed diagnostic while 88.36% of segments (n=94) with FLASH readouts were deemed diagnostic (**Figure 15**).

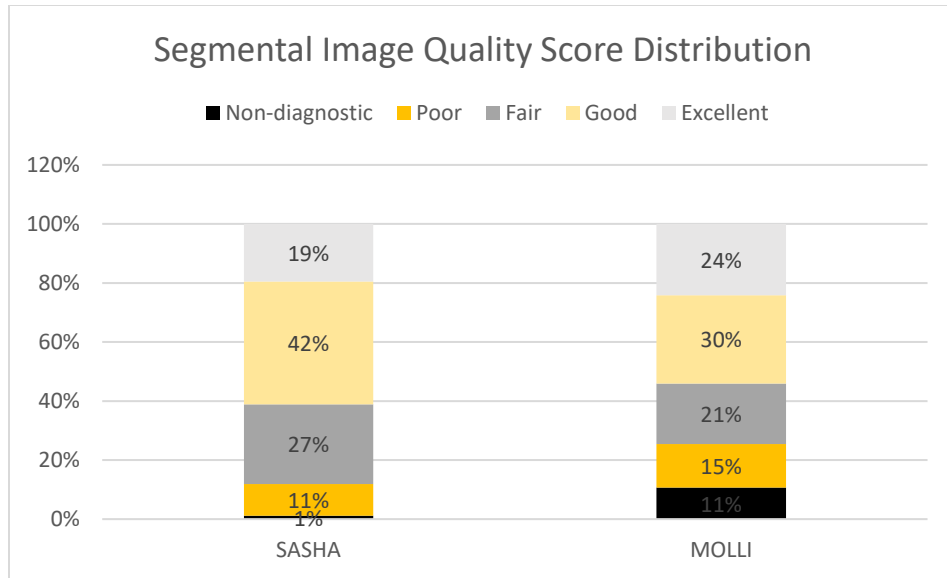


Figure 14. Image quality score distribution between SASHA and MOLLI segmental scans within the heart in pre-contrast values. Results are a combination of all readouts.

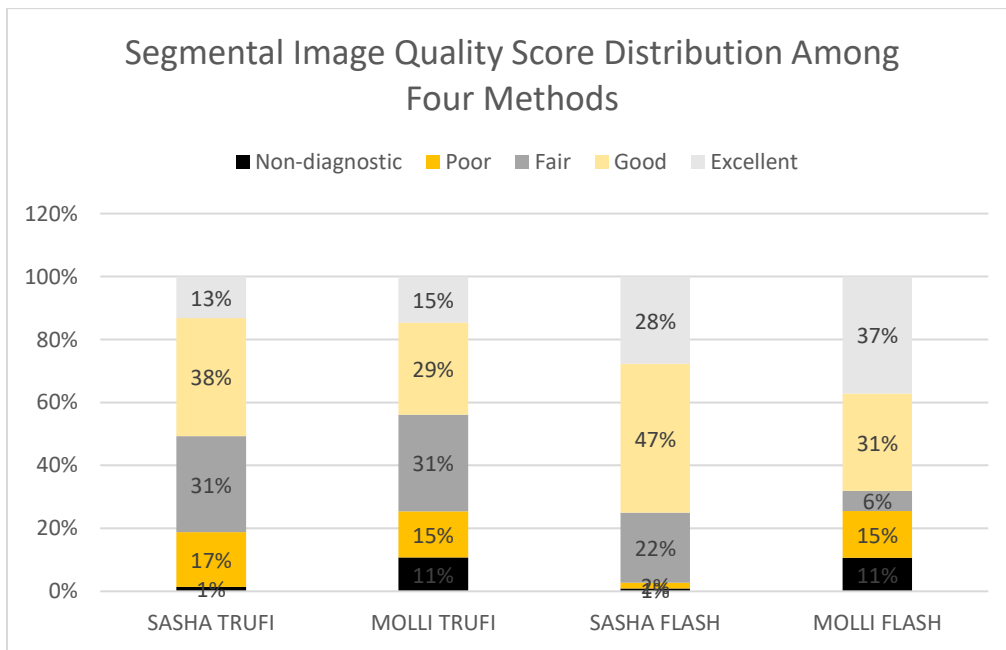


Figure 15. Distribution of segmental image quality scores among the four methods: SASHA TRUFI, MOLLI TRUFI, SASHA FLASH, and MOLLI FLASH in pre-contrast values.

In comparison of segmental values, MOLLI TRUFI demonstrated a significant difference in means between initial ($T1_{AVG}=756\pm194\text{ms}$) and secondary ($T1_{AVG}=828\pm175\text{ms}$) visits ($p\text{-value}=0.0000086$). Looking at the CoV of all segments among four participants, MOLLI showed higher CoV when compared to SASHA. Out of 216 segments across four participants, 59.26% of segments scanned with MOLLI had higher CoV. This indicates MOLLI having a higher variability in segmental, pre-contrast T1 values. When comparing the different readouts, segments with a TRUFI readout on average had a higher CoV when compared to FLASH.

Among segmental post-contrast values, 12% of MOLLI scans were deemed excellent compared to only 10% of SASHA scans (**Figure 16**). When looking at each method individually, SASHA FLASH had a lower percentage of segments deemed non-diagnostic at 1% in post-contrast values (**Figure 17**).

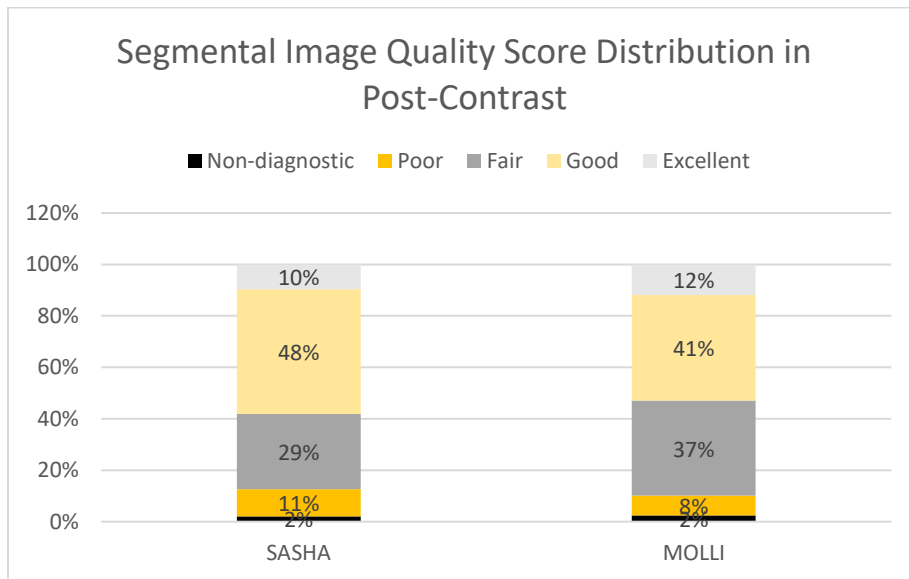


Figure 16. Image quality score distribution between SASHA and MOLLI segmental scans within the heart in post-contrast values.

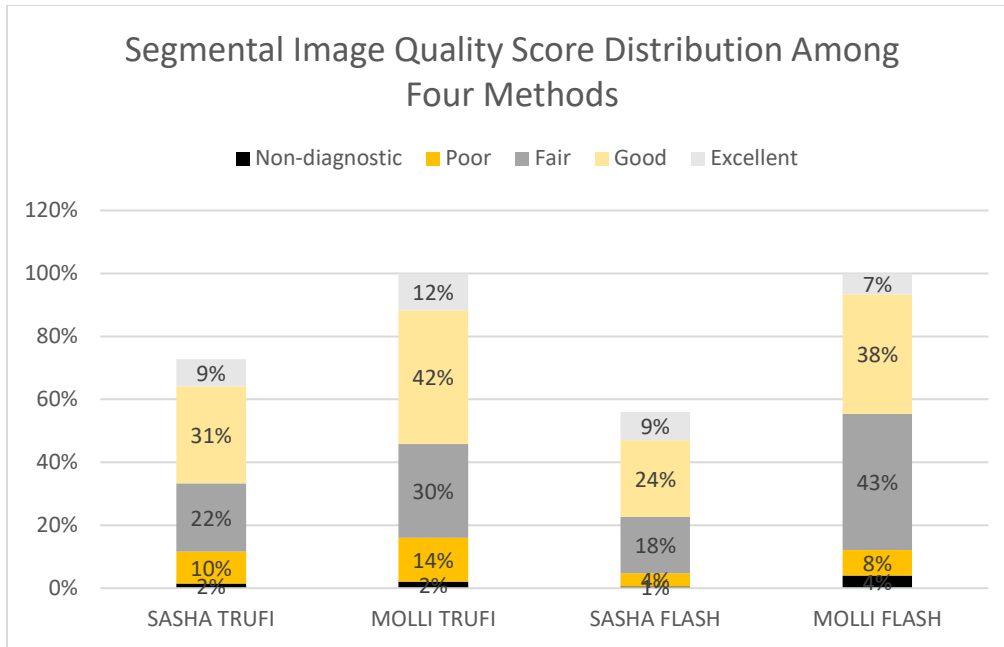


Figure 17. Distribution of segmental image quality scores among the four methods: SASHA TRUFI, MOLLI TRUFI, SASHA FLASH, and MOLLI FLASH in post-contrast values.

A one-factor ANOVA test was performed on all native segmental data. The test suggests there is significant difference between the means of the T1 values on a segmental level. Further post hoc analysis via Tukey-Kramer test shows that SASHA TRUFI+MOLLI TRUFI, SASHA FLASH+MOLLI TRUFI, and MOLLI TRUFI+MOLLI FLASH exceeded the critical value ($q_{crit}=3.67$, $df=191$) (**Figure 18, Figure 19** **Figure 17**).

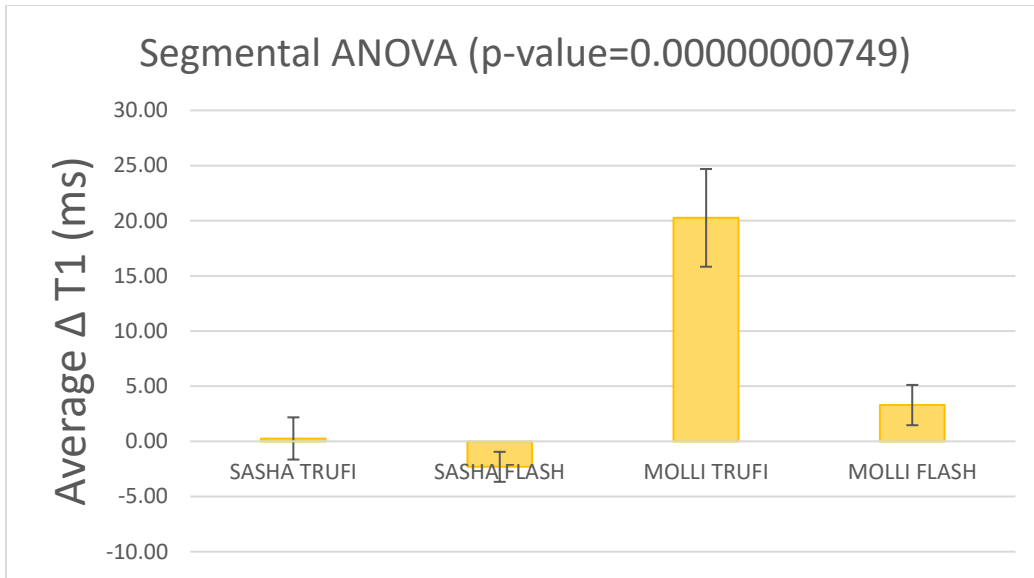


Figure 18. Graphical representation of segmental ANOVA results between SASHA TRUFI, SASHA FLASH, MOLLI TRUFI, and MOLLI FLASH in pre-contrast scans.

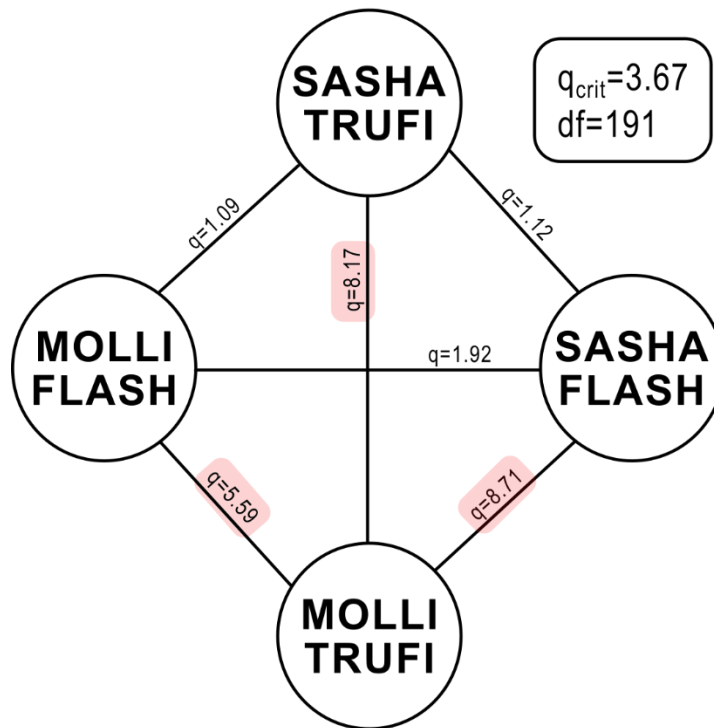


Figure 19. Tukey-Kramer results showing variations between the four methods and their q-values for segmental, native T1-values.

In post-contrast analysis, an ANOVA test shows statistically significant difference among the four groups. The post hoc test determined that MOLLI TRUFI+MOLLI FLASH were statistically different within the groups ($q_{crit}=3.67$, $df=151$) (**Figure 20**). The post-contrast analysis can highlight the discrepancies between scans and T1 values as the values decrease with contrast. This may have been enough to bring the differences between MOLLI TRUFI and MOLLI GRE to the surface whereas pre-contrast values could not show any significant differences.

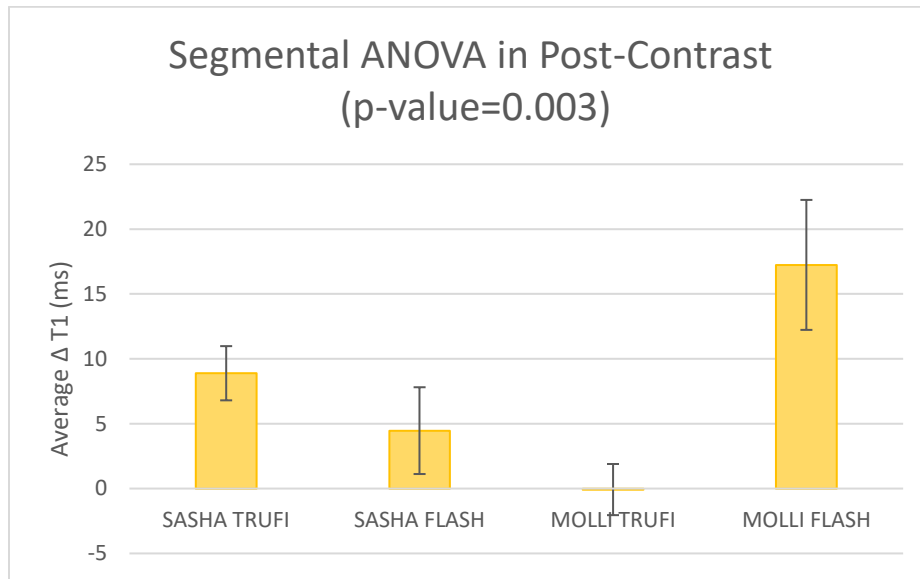


Figure 20. Graphical representation of segmental ANOVA results between SASHA TRUFI, SASHA FLASH, MOLLI TRUFI, and MOLLI FLASH in post-contrast scans.

In post contrast values, segments scanned with MOLLI showed higher CoV when compared to SASHA. The higher CoV affected the basal and mid-cavity slices. This may be due to the placement of the generator box of CIEDs near the area causing field inhomogeneities that highly affect MOLLI sequences (39, 43-45).

When compared to a slice-based analysis, it was interesting to note that MOLLI FLASH's mode shifted to a score of 3 (fair) in segmental analysis. In both ANOVA results, MOLLI TRUFI

contained significant statistical difference. This may indicate some trouble in using either the MOLLI sequence or TRUFI readout when scanning participants, especially those with CS and CIEDs.

3.3 T2 Considerations

In a slice-based analysis of T2 values among the available participants, those with a TRUFI readout showed a significant change in means in participants four and five (p-values: 0.001 and 0.041 respectively). Scans done with a FLASH readout revealed no significant difference between initial and secondary visits on a slice-based level.

In contrast, for initial and secondary segmental T2 values between visits, participants scanned with a FLASH readout consistently showed significant change in means: p-values = 0.0004, not available, 0.0002, and 0.0335 respectively for the four participants indicating a change in T2 means between visits.

Under a one-factor ANOVA analysis, there was no suggestion that there are significant differences between the means of the T2 delta values between the readout T2 map variants (**Figure 21, Figure 22**). Overall, the MOLLI GRE protocol may be more reproducible and considered for T2 acquisition.

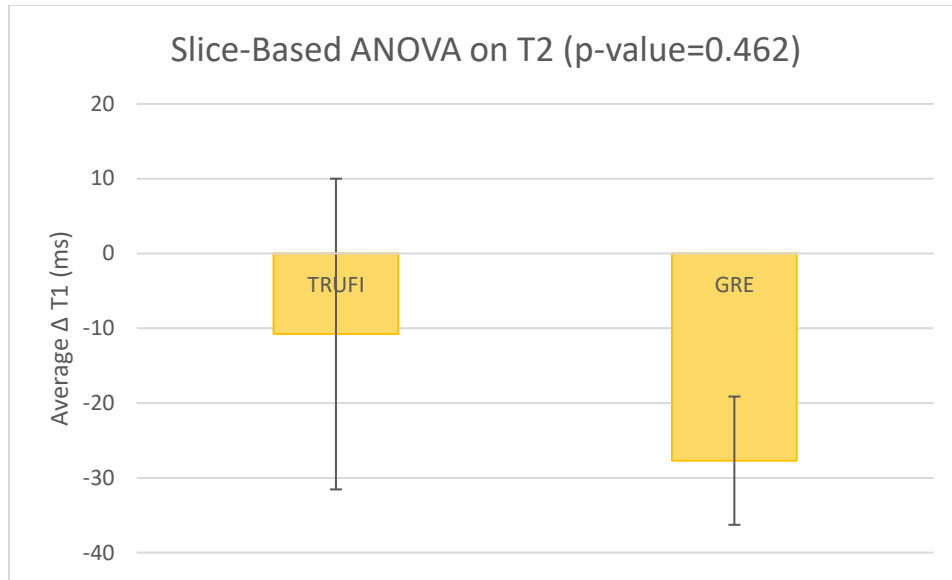


Figure 21. Graphical representation of slice-based ANOVA results between TRUFI and FLASH readouts using T2 values.

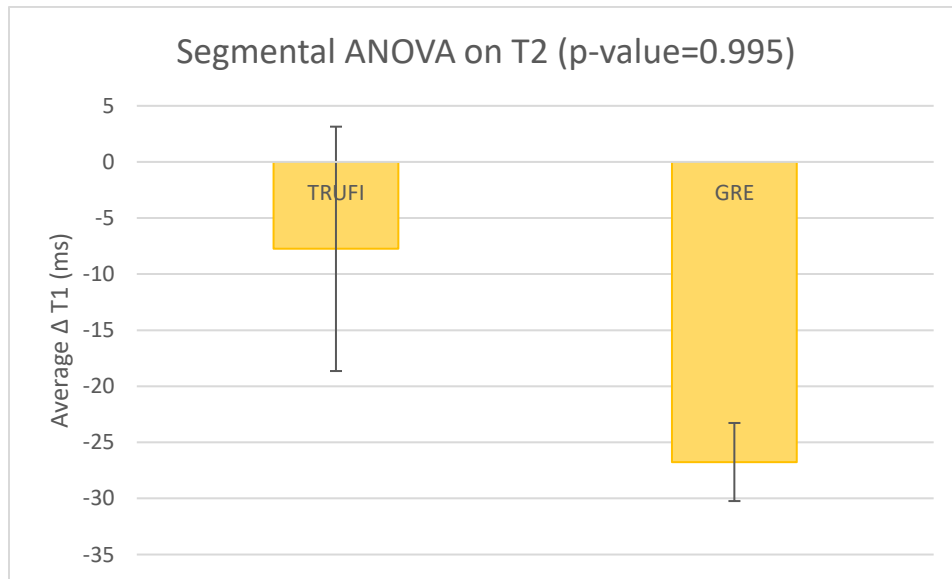


Figure 22. Graphical representation of segmental ANOVA results between TRUFI and FLASH readouts using T2 values.

3.4 An In-Depth Look: A Head-to-Head Comparison

Due to the nature of this study, each protocol was optimized with every consecutive patient. After the first participant's initial and secondary scans, the protocol was slightly revised and optimized before being

applied to the next participant and so on. As a result, it is reasonable to assume that the fifth participant was scanned with the most refined protocol. The fifth participant was also the only participant to have all four methods scanned and of diagnostic use. This may warrant an in-depth look at the scan data from a single patient in a head-to-head comparison of all four methods. IQS scores for the fifth participant were compiled. A paired t-test was applied to the initial and secondary visit T1 values. A single factor ANOVA test was also done on the delta values of each method.

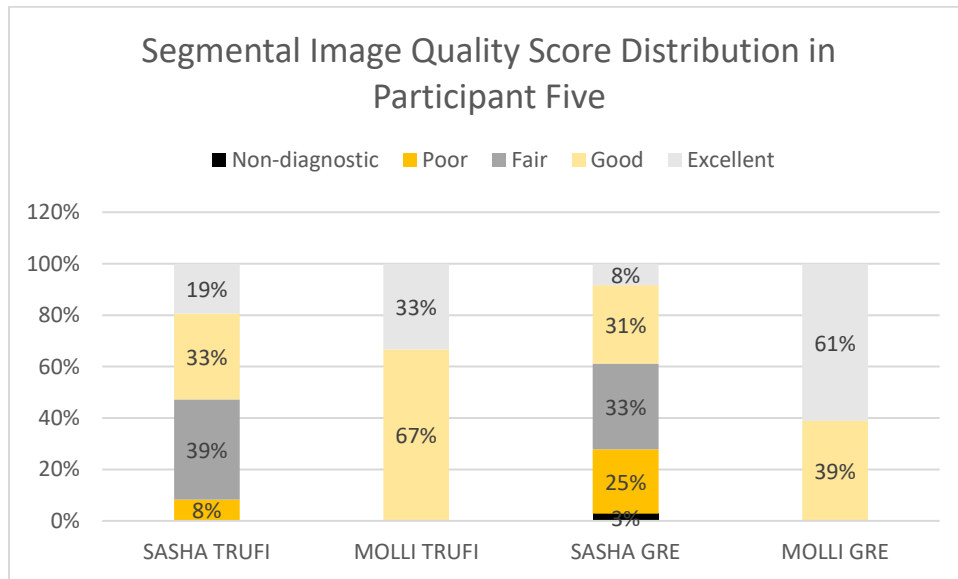


Figure 23. IQS scores for participant 5.

Only one segment was deemed non-diagnostic and removed from further statistical analysis. A paired t-test was performed on all initial and secondary visits. A single factor ANOVA test was done and did not find any statistically significant differences in the variances (p-value=0.663) (**Figure 24**). A Tukey-Kramer test was still performed to compare every combination to see how each result affected the overall variance. The only pairing that did not exceed the q_{crit} value was the pairing between MOLLI FLASH and SASHA FLASH (**Figure 25**).

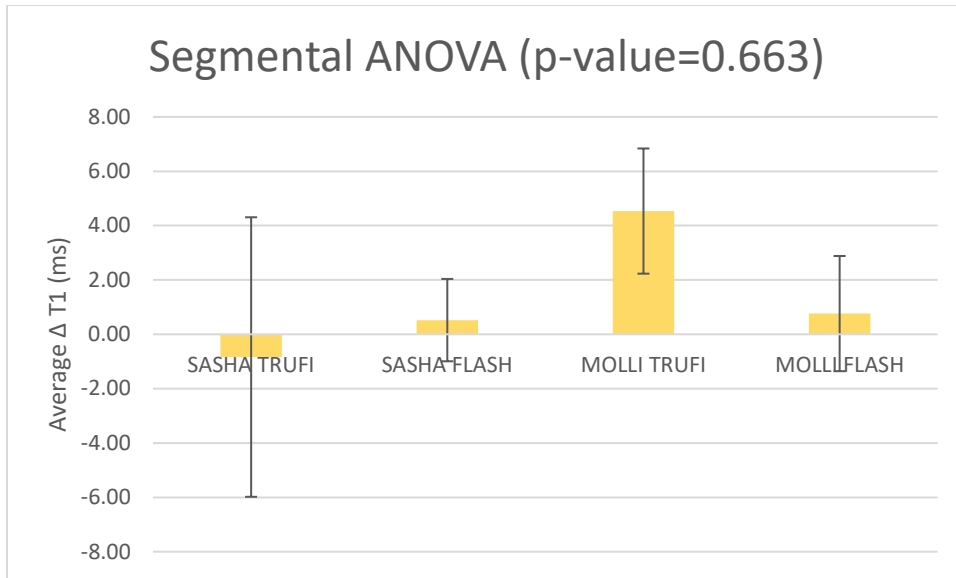


Figure 24. ANOVA results for participant five.

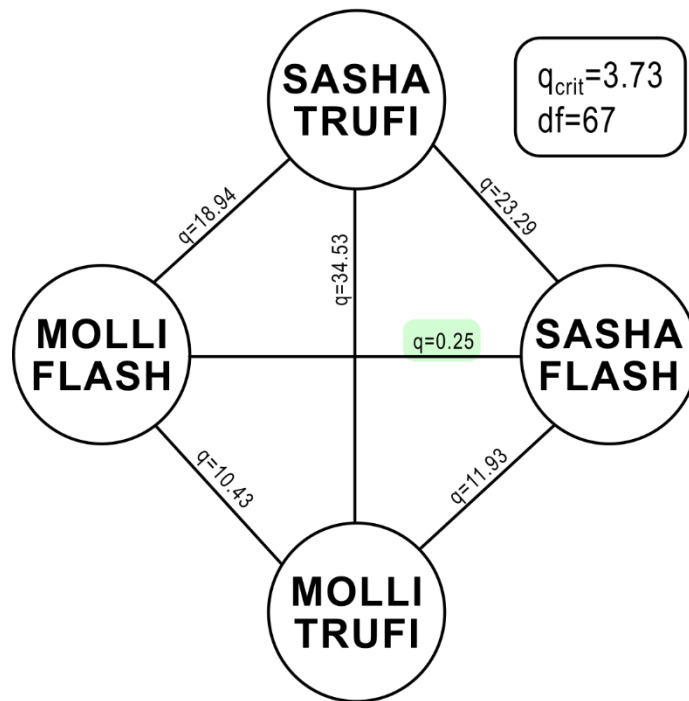


Figure 25. Tukey-Kramer results showing variations between the four methods and their q-values in participant five

Looking at the isolated participant, it may indicate that a FLASH readout is more reliable compared to the other combinations. Although a post-hoc analysis was not necessary, it revealed that MOLLI FLASH and

SASHA FLASH were the only to have an agreeable mean. This may indicate that FLASH has lower variance compared to the other methods (**Figure 25**).

3.5 Future Directions

CMR continues to display its benefits in non-invasive imaging for patients with sarcoidosis and CIEDs. As these patients may be considered difficult to image, this study attempts to find a reliable scanning sequence which is able to accurately define focal and diffuse fibrosis with consistent results when repeated. Although inversion recovery methods like MOLLI are well documented, exploring saturation recovery methods like SASHA may offer promising results in the presence of diffuse fibrosis and artifact from devices. Future studies should further investigate the benefit of using a saturation recovery method with a FLASH readout to assess sarcoidosis patients more accurately for research and clinical management.

Although the type of scanning sequence is an important choice in regard to scanning patients with challenging imaging circumstances, like sarcoidosis and CIEDs, the added complexity of readout choice will also play a role in optimizing applications for clinical or research settings. While the need for a non-biomarker method of monitoring or detecting sarcoidosis increases, CMR continues to make strides to fulfill that role. CMR's potential for non-invasive and non-ionizing imaging is growing, and its integration of qualifiable and quantifiable data will prove useful in research and clinical settings. By optimizing a CMR protocol for CS patients with devices, a key barrier is overcome in obtaining clinically useful imaging for disease monitoring and diagnosis.

4 References

1. Mahesh M. The Essential Physics of Medical Imaging, Third Edition. Med Phys. 2013;40(7).
2. Gruber B, Froeling M, Leiner T, Klomp DWJ. RF coils: A practical guide for nonphysicists. J Magn Reson Imaging. 2018.
3. Bloch F. The Principle of Nuclear Induction. Science. 1953;118(3068):425-30.
4. Rohrer M, Bauer H, Mintorovitch J, Requardt M, Weinmann HJ. Comparison of magnetic properties of MRI contrast media solutions at different magnetic field strengths. Invest Radiol. 2005;40(11):715-24.
5. Elster AD. How much contrast is enough?. Dependence of enhancement on field strength and MR pulse sequence. Eur Radiol. 1997;7 Suppl 5:276-80.
6. Abdel-Aty H, Boyé P, Zagrosek A, Wassmuth R, Kumar A, Messroghli D, et al. Diagnostic performance of cardiovascular magnetic resonance in patients with suspected acute myocarditis: comparison of different approaches. J Am Coll Cardiol. 2005;45(11):1815-22.
7. Fazel R, Krumholz HM, Wang Y, Ross JS, Chen J, Ting HH, et al. Exposure to low-dose ionizing radiation from medical imaging procedures. N Engl J Med. 2009;361(9):849-57.
8. Einstein AJ. Effects of radiation exposure from cardiac imaging: how good are the data? J Am Coll Cardiol. 2012;59(6):553-65.
9. Wilk B, Wisenberg G, Dharmakumar R, Thiessen JD, Goldhawk DE, Prato FS. Hybrid PET/MR imaging in myocardial inflammation post-myocardial infarction. J Nucl Cardiol. 2020;27(6):2083-99.
10. Friedrich MG, Marcotte F. Cardiac magnetic resonance assessment of myocarditis. Circ Cardiovasc Imaging. 2013;6(5):833-9.
11. Quarta G, Holdright DR, Plant GT, Harkness A, Hausenloy D, Hyare H, et al. Cardiovascular magnetic resonance in cardiac sarcoidosis with MR conditional pacemaker in situ. J Cardiovasc Magn Reson. 2011;13:26.
12. Tada Y, Yang PC. Myocardial Edema on T2-Weighted MRI: New Marker of Ischemia Reperfusion Injury and Adverse Myocardial Remodeling. Circ Res. 2017;121(4):326-8.
13. Rahsepar AA, Collins JD, Knight BP, Hong K, Carr JC, Kim D. Wideband LGE MRI permits unobstructed viewing of myocardial scarring in a patient with an MR-conditional subcutaneous implantable cardioverter-defibrillator. Clin Imaging. 2018;50:294-6.
14. Diao KY, Yang ZG, Xu HY, Liu X, Zhang Q, Shi K, et al. Histologic validation of myocardial fibrosis measured by T1 mapping: a systematic review and meta-analysis. J Cardiovasc Magn Reson. 2016;18(1):92.
15. de Meester de Ravenstein C, Bouzin C, Lazam S, Boulif J, Amzulescu M, Melchior J, et al. Histological Validation of measurement of diffuse interstitial myocardial fibrosis by

myocardial extravascular volume fraction from Modified Look-Locker imaging (MOLLI) T1 mapping at 3 T. *J Cardiovasc Magn Reson.* 2015;17:48.

16. Bull S, White SK, Piechnik SK, Flett AS, Ferreira VM, Loudon M, et al. Human non-contrast T1 values and correlation with histology in diffuse fibrosis. *Heart.* 2013;99(13):932-7.

17. Vassiliou VS, Wassilew K, Cameron D, Heng EL, Nyktari E, Asimakopoulos G, et al. Identification of myocardial diffuse fibrosis by 11 heartbeat MOLLI T. *MAGMA.* 2018;31(1):101-13.

18. Kitterer D, Latus J, Henes J, Birkmeier S, Backes M, Braun N, et al. Impact of long-term steroid therapy on epicardial and pericardial fat deposition: a cardiac MRI study. *Cardiovasc Diabetol.* 2015;14:130.

19. Ise T, Hasegawa T, Morita Y, Yamada N, Funada A, Takahama H, et al. Extensive late gadolinium enhancement on cardiovascular magnetic resonance predicts adverse outcomes and lack of improvement in LV function after steroid therapy in cardiac sarcoidosis. *Heart.* 2014;100(15):1165-72.

20. Bing R, Dweck MR. Myocardial fibrosis: why image, how to image and clinical implications. *Heart.* 2019;105(23):1832.

21. Moon JC, Messroghli DR, Kellman P, Piechnik SK, Robson MD, Ugander M, et al. Myocardial T1 mapping and extracellular volume quantification: a Society for Cardiovascular Magnetic Resonance (SCMR) and CMR Working Group of the European Society of Cardiology consensus statement. *J Cardiovasc Magn Reson.* 2013;15:92.

22. Hilbert S, Weber A, Nehrke K, Börnert P, Schnackenburg B, Oebel S, et al. Artefact-free late gadolinium enhancement imaging in patients with implanted cardiac devices using a modified broadband sequence: current strategies and results from a real-world patient cohort. *Europace.* 2018;20(5):801-7.

23. Bhuva AN, Kellman P, Graham A, Ramlall M, Boubertakh R, Feuchter P, et al. Clinical impact of cardiovascular magnetic resonance with optimized myocardial scar detection in patients with cardiac implantable devices. *Int J Cardiol.* 2019;279:72-8.

24. Bhuva AaRMaBRaKKaFPaSNaSRaKPaMJaMC. 014 Wideband free breathing MOCO LGE changes patient care in patients with implantable cardiac defibrillators. *Heart.* 2017;103:A11-A2.

25. Singh A, Kawaji K, Goyal N, Nazir NT, Beaser A, O'Keefe-Baker V, et al. Feasibility of Cardiac Magnetic Resonance Wideband Protocol in Patients With Implantable Cardioverter Defibrillators and Its Utility for Defining Scar. *Am J Cardiol.* 2019;123(8):1329-35.

26. Stevens SM, Tung R, Rashid S, Gima J, Cote S, Pavez G, et al. Device artifact reduction for magnetic resonance imaging of patients with implantable cardioverter-defibrillators and ventricular tachycardia: late gadolinium enhancement correlation with electroanatomic mapping. *Heart Rhythm.* 2014;11(2):289-98.

27. Markl M, Leupold J. Gradient echo imaging. *J Magn Reson Imaging.* 2012;35(6):1274-89.

28. Bieri O, Scheffler K. Fundamentals of balanced steady state free precession MRI. *J Magn Reson Imaging*. 2013;38(1):2-11.
29. Carr HY. Steady-State Free Precession in Nuclear Magnetic Resonance. *Physical Review*. 1958;112(5):1693-701.
30. Huang TY, Huang IJ, Chen CY, Scheffler K, Chung HW, Cheng HC. Are TrueFISP images T2/T1-weighted? *Magn Reson Med*. 2002;48(4):684-8.
31. Scheffler K, Hennig J. Is TrueFISP a gradient-echo or a spin-echo sequence? *Magn Reson Med*. 2003;49(2):395-7.
32. Nazarian S, Cantillon DJ, Woodard PK, Mela T, Cline AM, Strickberger AS, et al. MRI Safety for Patients Implanted With the MRI Ready ICD System: MRI Ready Study Results. *JACC Clin Electrophysiol*. 2019;5(8):935-43.
33. Lynch JP, Hwang J, Bradfield J, Fishbein M, Shivkumar K, Tung R. Cardiac involvement in sarcoidosis: evolving concepts in diagnosis and treatment. *Semin Respir Crit Care Med*. 2014;35(3):372-90.
34. Ferreira VM, Schulz-Menger J, Holmvang G, Kramer CM, Carbone I, Sechtem U, et al. Cardiovascular Magnetic Resonance in Nonischemic Myocardial Inflammation: Expert Recommendations. *J Am Coll Cardiol*. 2018;72(24):3158-76.
35. Cooper MA, Nguyen TD, Spincemaille P, Prince MR, Weinsaft JW, Wang Y. How accurate is MOLLI T1 mapping in vivo? Validation by spin echo methods. *PLoS One*. 2014;9(9):e107327.
36. Birnie DH, Sauer WH, Bogun F, Cooper JM, Culver DA, Duvernoy CS, et al. HRS expert consensus statement on the diagnosis and management of arrhythmias associated with cardiac sarcoidosis. *Heart Rhythm*. 2014;11(7):1305-23.
37. Kellman P, Wilson JR, Xue H, Ugander M, Arai AE. Extracellular volume fraction mapping in the myocardium, part 1: evaluation of an automated method. *J Cardiovasc Magn Reson*. 2012;14:63.
38. Cerqueira MD, Weissman NJ, Dilsizian V, Jacobs AK, Kaul S, Laskey WK, et al. Standardized myocardial segmentation and nomenclature for tomographic imaging of the heart. A statement for healthcare professionals from the Cardiac Imaging Committee of the Council on Clinical Cardiology of the American Heart Association. *Circulation*. 2002;105(4):539-42.
39. Roujol S, Weingärtner S, Foppa M, Chow K, Kawaji K, Ngo LH, et al. Accuracy, precision, and reproducibility of four T1 mapping sequences: a head-to-head comparison of MOLLI, ShMOLLI, SASHA, and SAPPHIRE. *Radiology*. 2014;272(3):683-9.
40. McDiarmid AK, Broadbent DA, Higgins DM, Swoboda PP, Kidambi A, Ripley DP, et al. The effect of changes to MOLLI scheme on T1 mapping and extra cellular volume calculation in healthy volunteers with 3 tesla cardiovascular magnetic resonance imaging. *Quant Imaging Med Surg*. 2015;5(4):503-10.

41. Bhuva AN, Nordin S, Bulluck H, Treibel TA, Abdel-Gadir A, Rosmini S, et al. Reproducibility of native T1 mapping using ShMOLLI and MOLLI - implications for sample size calculation. *Journal of Cardiovascular Magnetic Resonance*. 2016;18(Suppl 1):P2.
42. Lin K, Suwa K, Ma H, Collins JD, Markl M, Carr JC. Variability of native T1 values: implication for defining regional myocardial changes using MRI. *Int J Cardiovasc Imaging*. 2018;34(10):1637-45.
43. Child N, Suna G, Dabir D, Yap ML, Rogers T, Kathirgamanathan M, et al. Comparison of MOLLI, shMOLLI, and SASHA in discrimination between health and disease and relationship with histologically derived collagen volume fraction. *Eur Heart J Cardiovasc Imaging*. 2018;19(7):768-76.
44. Tirkes T, Zhao X, Lin C, Stuckey AJ, Li L, Giri S, et al. Evaluation of variable flip angle, MOLLI, SASHA, and IR-SNAPSHOT pulse sequences for T. *MAGMA*. 2019;32(5):559-66.
45. Robson MD, Piechnik SK, Tunnicliffe EM, Neubauer S. T1 measurements in the human myocardium: the effects of magnetization transfer on the SASHA and MOLLI sequences. *Magn Reson Med*. 2013;70(3):664-70.